Project No. R19513P
Date: January 9, 2023
Humboldt, Saskatchewan

Pneumatic Grain Conveying in Seeding Equipment

TECHNICAL REPORT

Submitted To: **Manitoba Agriculture**
Winnipeg, Manitoba

Saskatchewan Canola Development Commission
Saskatoon, Saskatchewan

Submitted By: Ian Paulson, P.Eng. M.Sc.
Technical Services Lead

Charley Sprenger, B.E., M.Sc.
Project Leader

Justin Gerspacher, Engineer-In-Training
Project Engineer

TABLE OF CONTENTS

1. EXECUTIVE SUMMARY

Air drills continue to be a popular choice for seeding many of the crops grown in the prairies today. Air drill development has continued since their invention in the 1980s, but the core of many modern air drills, the pneumatic conveying system, still relies on the passive division of seed through well-mixed, two-phase (gas-solid) flows.

Many factors are known to influence the distribution consistency of passive solid-gas flow division. In the context of air drills, these factors include distributor geometry, fan speed, primary and secondary hose lengths and routings, and machine orientation while in operation. The implications of these complex system interactions were lacking discussion in the literature.

The physical testing and validation of these systems is known to be labour intensive, particularly for a full-scale machine. However, advancements in modern computing capacity and available simulation tools have put the investigation of these systems and the development of operational best practices by means of numerical modeling methods within reach of the industry. Specifically, computational fluid dynamics (CFD) modeling has been used in the literature to simulate the behaviour of fluid flowing in pipes and hoses, including some published applications to agricultural pneumatic conveying. The discrete element method (DEM) is a computation method for simulating the movement and behaviour of individual (discrete) particles in granular flows. Recent developments in computational coupling schemes now enable one to simulate the response of granular particles in the presence of dynamic fluid flow fields.

In the broader context of the project, the three objectives were to

- determine the effect of air velocities, air hose lengths and routing geometries, and/or tool bar angles on the seed distribution coefficient of variance (CV) and germination of canola in a pneumatic conveying system,
- develop and validate numerical models CFD-DEM models to track machine-seed interactions, and
- train one highly qualified person (HQP) in the field of numerical simulation and equipment validation to optimize air seeder performance.

To investigate the relationship between seed distribution consistency and various parameters related to the pneumatic conveying system of an air drill, experiments were conducted on a John Deere 1870 double-shoot hoe drill and 1910 air cart. Air velocity and static pressure were measured in the primary hoses, and a subset of the secondary hoses. Hose lengths and routing geometry were measured as part of characterizing the equipment. Hose lengths were used in the subsequent data analysis, and the hose geometry supported the development of numerical models. Air flow measurements were taken with and without seed being conveyed. Three different fan speed treatments were used (2,200, 2,800, and 3,400 RPM), and three replications of each treatment were completed.

Seed germination was also measured after the experiments were completed to characterize possible germination effects from pneumatic conveying; samples were grouped by distributor and fan speed treatment. InVigor® L233P seed was used for all conveying experiments.

Within-opener variation between runs, CV1, ranged from 0.52% to 0.71% with no strong dependency on fan speed. However, variation between openers (CV2) did increase with fan speed, ranging from 10.74% at 2,200 RPM to 12.57% at 3,400 RPM. The lowest fan speed (2,200 RPM) was the fan speed suggested by the operator's manual for the seed type and mass flow rate under consideration. Thus, for this air cart/drill combination under the given operating conditions, it was concluded that increasing the fan speed beyond what was suggested by the operator's manual would needlessly decrease distribution uniformity while likely increasing hydraulic power consumption and the risk of seed bouncing out of the soil furrow. The six primary hoses/distributors were numbered from left to right of the air drill looking forward. The average variation within distributors (CV3) ranged between a minimum of 7.7% for distributor 2 and maximum of 12.1% for distributor 4; distributor 3 was excluded from comment due to the outsized CV3 value that resulted from debris becoming lodged in the distributor during testing. Further analysis indicated that within-distributor variance significantly increased with increased fan speed. This further strengthens the conclusion that, for the conditions tested, operating with a fan speed greater than that suggested by the operator's manual was detrimental to the consistency of seed distribution across the air drill.

A linear statistical model including the factors fan speed, distributor number, and secondary position, secondary hose length, and their interaction, was developed for the response variable of normalized seed mass per opener (not CV). A statistically significant model was fit ($R^2_{adjusted}$ = 0.821), where distributor number, and secondary position, secondary hose length, and their interaction were statistically significant, but fan speed was expectedly not significant. Secondary hose position 1 aligned with the incoming primary hose and numbering proceeded clockwise viewed from above. Several conclusions were made from the results of this model. Longer secondary hoses received less seed, which suggests an influence of secondary hose length on the dividing characteristics of a distributor. Seed distribution was influenced by the angular position of the secondary hoses, which suggests a structural inconsistency in the division of seed among the distributor outlets. Additionally, the significant interaction term between secondary hose length and position factors imply some secondary positions were more sensitive to hose lengths.

Static pressure results were largely in line with expectations; however, stronger symmetry was expected. Primary hose length effects were evident from the notably lower static pressure values for primary hoses 3 and 4. As all primary hoses are "coupled" via the common plenum at the fan, hoses that present a lower resistance should see increased airflow through them, with all other factors held equal.

The measured air speed results in the primary hoses provided as much characterization of the differences in air velocity in the primary hoses as they did a commentary on the variation of airspeed across the diameter of the primary and the sensitivity of pitot tube placement. However, the differences noted in the velocity in the primary hoses was greater than the uncertainty contribution expected from potential pitot tube placement error. Based on this, it is suggested that the assumption of fully developed flow with the maximum velocity occurring at the centerline of the pipe is an overly ideal simplification of the flow behaviour throughout much of a typical pneumatic conveying system. Air velocity was also difficult to reliably measure in the secondary hoses.

Finally, a small but detectable increase in static pressure due to canola being conveyed in the primary hoses occurred (1.59% to 3.21% increase above the air-only values). At these small solids loading ratios (SLRs), ranging between approximately 0.038 and 0.059, the impact of fan speed was much larger than that of canola being conveyed.

Laboratory testing was conducted using a single-hose pneumatic conveying apparatus that terminated in a J-tube and distributor with eight secondary hose outlets; testing was conducted by the project HQP at the University of Saskatchewan. The impact of secondary hose length on various quantities including seed mass distribution was investigated with four different configurations of secondary hose length. Equal length secondary hoses were tested, as well as configurations with increased hose lengths secondary 5, secondaries 5 and 6, and finally secondaries 5 to 7. The impact of closed outlets was also investigated, first by blocking the entry to secondary hose 5, then secondary hoses 5 and 6. The average air velocity in the primary hose was varied between 13 and 20 m/s, with a fixed seed mass flow rate of 0.0031 kg/s.

CV ranged between 9.32% and 10.36% and increased with air speed. These CV values were similar to the values measured during full-scale air drill testing. Overall, the greatest seed mass fraction flowed through secondary hose 1, while position 6 typically had the lowest mass fraction (despite position 5 being diametrically opposite position 1 as this distributor had eight outlets). This slight shift could be due to swirl occurring within the vertical portion of the J-tube and into the distributor. To a small degree, increasing the length of the secondary hose tended to reduce the proportion of seed that was delivered through that hose, although the impact became less clear as more hoses were lengthened. Blocking secondary outlets tended to redistribute the flow of seed to outlets immediately beside the blockage.

Overall, these lab experiments provided a data collection environment that permitted specific and controlled changes to hose geometries and operating conditions to support further study and model validation efforts. The presence of several trends that were also evident when testing a full-scale drill made by a different manufacturer was encouraging, as the understanding and overall conclusions of the project can be assumed to extend beyond a specific make and model of air drill.

Simulating the pneumatic conveying of canola through an air drill began with the development of an air-only CFD model of a primary hose, and eventually a distributor and secondary hoses. The predicted pressure drop was somewhat higher than some experimental results but, in general, the results agreed well with available validation data. Flow separation occurred on the inside of the J-tube elbow even at the lowest fan speed replicated in the simulation, leading to higher-velocity air flowing around the outside of the elbow. However, the dimples in the vertical portion of the J-tube did aid in reducing the asymmetry of the velocity profile. Regardless, a structural imbalance of the mass flow rate of air existed. Regardless of the simulated fan speed, more air flowed through the secondary hoses opposite the side of the J-tube elbow, with the mass flow rate evenly transitioning to the lowest rate through secondary hose 1.

Modifying the length of the secondary hoses resulted in a shift in air mass flux away from lengthened hoses (20.8% longer) toward shortened hoses (25.4% shorter). This bias was basically additive to the underlying imbalance present between secondary outlets on the inside versus the outside of the elbow. The ratio of maximum to minimum air mass fraction values increased from 1.06 with equal length secondary hoses to 1.22 with unequal length hoses.

The parameters developed through the equal and unequal length secondary hose simulations were used to create a CFD model to represent the full-scale air drill used during testing, based on measurements taken during the testing period. The impact of the routing of primary hoses was apparent from those simulations, as was the impact of the large variation of secondary hose lengths and their positions within the distributors. High-curvature bends immediately upstream of the entry to the J-tube, like that present in primary hose 4, affected the flow pattern within the J-tube. Conversely, the disturbance from gentle bends further from the J-tube were smoothed out if sufficient distance was provided upstream of the J-tube elbow.

The flow field results were then used with a one-way coupling scheme to simulate the movement of canola particles using the discrete element method. One-way coupling enabled relevant lift and drag aerodynamic forces to be transferred onto each particle in the simulation, but the presence of the canola particles did not affect the airflow solution. Within the DEM simulations, collisions between particles and with walls were modeled.

The pattern of seed mass distribution for a distributor with equal length hoses was similar to the single-hose lab results. However, the simulated results indicated a greater difference between the maximum seed mass flow through secondary position 1 and minimum seed mass flow through the secondary hoses opposite position 1 (positions 5 and 6). Seed was typically carried along the outside of the J-tube elbow before impacting the first dimple. Seeds then either

1. bounced between opposite sides of the vertical tube and preferentially entered secondary hose 1 and its neighbors, or
2. were re-entrained into the airflow but were unable to follow the highest velocity air flow through secondary hoses 5 and 6.

Altering the length of some secondary hoses resulted in significantly less variation in the seed mass flow rate between position 1 and position 5 or 6. Notably, there was not a strong bias in seed flow specifically toward the shorter hoses in these simulations. Qualitatively, this only partially agreed with the results from the single-hose laboratory testing, but more study is warranted. In contrast to the experimental results of the project, increasing the air velocity did not have a noticeable impact on the distribution consistency with either equal or unequal length secondary hoses.

In simulations of the air drill used during full-scale testing, there was an observed trend between increased secondary hose length and both decreased air and seed mass fluxes. This was clearer in primary hose 6 compared to primary hose 4, as a large bend was present upstream of the entry into the J-tube of distributor 4, which made this trend less clear.

This project represented a multi-year effort in measuring air drill distribution performance, both in the laboratory and at full scale, in addition to simulating various configurations of pneumatic conveying systems. While several themes from the results point to opportunities for improved design of these systems, within the confines of existing machines the project ultimately highlighted the importance of simple but careful maintenance of air drill pneumatic conveying components and systems.

Consistent secondary hose lengths and resulting pressure drops are important to system performance; however, the interaction between secondary hose length and outlet position is complex. Therefore, the manufacturer suggested hose routings should be followed unless actual performance data suggest otherwise. If seed distribution consistency is in doubt, verifying the actual performance of a drill in the range of operation actually employed by an operator is a small cost, particularly when weighed against modern input commodity prices.

Severe bends should be minimized in both primary and secondary hoses as much as possible. Introducing sharp bends close to the entry of a J-tube elbow should be avoided when replacing primary hoses. Furthermore, the hose fastening/restraint schemes suggested by manufacturers should be used. Replace damaged or kinked hoses immediately.

In the range of SLRs tested (relatively low when compared to most other seed and fertilizers) with the equipment studied in this project, increasing the fan speed actually worsened the distribution consistency, as opposed to improving it by “promoting more mixing” as is sometimes anecdotally suggested. In the simulation results, distribution consistency was at least no better when the air velocity increased. In the testing conducted in this project, the manufacturer-suggested fan speed provided the most consistent distribution of seed across the air drill. Furthermore, the air mass distribution was generally quite consistent across the range of fan speeds tested for the air drill geometries considered throughout this work. Unless drill-specific information suggests otherwise, the most appropriate fan speed is the one suggested by the manufacturer.

Finally, pneumatic conveying the canola variety used under the conditions tested through the particular air drill used during full-scale testing did not result in a reduction in germination from the control sample, and significant variations in samples taken across the air drill after conveying were not evident.

The data and results developed through the course of this project indicated several opportunities for future work. The reduction in the difference between minimum and maximum seed mass fractions that resulted from unequal secondary hose lengths was surprising; a closer mirroring of the air mass fraction response was expected. A detailed analysis of particle trajectories through the asymmetric flow fields may highlight the mechanism(s) that tended to "smooth out" the front-rear seed distribution.

The data suggest that more optimal hose routings (both primary and secondary) are possible, even within the constraints of current designs. Tight bends in both primary and secondary hoses had an apparent impact on distribution consistency. However, given the complex interaction between secondary hose lengths and positions, improvements should be sought via engineered changes developed by manufacturers; owner/operator modifications are not recommended.

Machinery bouncing and accelerations were not considered, as all testing and simulation results reflected stationary equipment. An investigation through bench-scale testing or by incorporating motion into simulations is suggested as a first step.

Further study of particle-wall DEM interaction parameters that reflect used machinery across a wide range of repair is warranted, as well as particle-particle DEM interaction parameters specific to seeding scenarios including on-farm or in-field applied seed treatments.

2. ACKNOWLEDGEMENTS

This Project was made possible by funding from the Governments of Manitoba and Canada through the Canadian Agricultural Partnership, as well as through contributions from the Saskatchewan Canola Development Commission.

Additionally, the authors would like to acknowledge the efforts and contributions of the M.Sc. student involved with the project, Sarita Victoria Casas Urrunaga, supervising faculty Professors Donald Bergstrom and Scott Noble, and the Mechanical Engineering Department at the University of Saskatchewan through the use of the Air Handling Laboratory.

3. INTRODUCTION

Initially developed in western Canada in the 1980s, air drills continue to be a popular choice for seeding many of the crops grown in Manitoba and Saskatchewan today. Air drill engineering development has continued since their introduction to the region, with modern air drills employing sectional control, turn compensation, variable rate control, blockage monitoring, independent row units, down-pressure adjustment features, and many other manufacturer-specific enhancements. However, the core of many modern air drills, the pneumatic conveying system, still relies on the passive division of input products (i.e., seed, fertilizer) through a well-mixed two-phase (gas-solid) flow.

Many factors are known to influence the main performance metric, distribution consistency, of passive solid-gas flow division. In the context of air drills, these factors potentially include distributor geometry and orientation, fan speed, primary and secondary hose lengths and their routings, and machine/component spatial orientations while operating in the field. Some of these factors have been studied in the open literature, but the discussion of their impact in the context of a full-scale air drill is less prevalent. The operational implications of these complex system interactions are also lacking in the literature.

The physical testing and validation of these systems is known to be labour intensive, particularly for a full-scale machine. However, advancements in modern computing capacity and available simulation tools have put the investigation of these systems and the development of operational best practices by means of numerical modeling methods within reach of the industry. Specifically, computational fluid dynamics (CFD) modeling has been used in the literature to simulate the behaviour of fluid flowing in pipes and hoses, including some published applications to agricultural pneumatic conveying. The discrete element method (DEM) is a computation method for simulating the movement and behaviour of individual (discrete) particles in granular flows. Recent developments in computational coupling schemes now enable one to simulate the response of granular particles in the presence of fluid flow fields.

In the broader context of the project, the three objectives were to

- determine the effect of air velocities, air hose lengths and routing geometries, and/or tool bar angles on the seed distribution coefficient of variance (CV) and germination of canola in a pneumatic seeding system,
- develop and validate numerical models CFD-DEM models to track machine-seed interactions, and
- train one HQP in the field of numerical simulation and equipment validation to optimize air seeder performance.

With these objectives in mind, a review of the research literature related to experimental testing and numerical modeling of pneumatic conveying research is presented in **Section 3**. In **Section 5**, activities related to the testing of a full-scale air drill to quantify seed damage, seed distribution consistency, and air flow behaviour is presented. Experimental work on a lab-scale single-hose

pneumatic conveying system performed by the graduate student involved in this project is summarized in **Section 5**. The development of numerical model to predict both the airflow behaviour and the seed distribution performance of several configurations of pneumatic conveying systems is presented in **Section 6**. In **Section 7**, the impact to operational practices gleaned from the results of the project are discussed. Finally, opportunities for future work are discussed in **Section 8**.

4. LITERATURE REVIEW

The existing literature were reviewed in regard to air seeder configurations and functionality, experimental pneumatic conveying research, and numerical modeling related to pneumatic conveying.

4.1 Experimental Pneumatic Conveying Research

The transportation of solid particles via a pressurized fluid media, commonly referred to as pneumatic conveying, is a method commonly used in many industries. A wide range of products can be conveyed using this approach, from fine powders (Ratnayake, 2017) to large seeds associated with agricultural air seeders, such as chickpeas. Pneumatic conveying systems are typically characterized by the operating pressure regime (positive or negative) and the solid loading ratio, which is the ratio of solid particle mass flow rate to the gas mass flow rate (Mills, 2016). Klinzing, Rizk, Marcus, & Leung (2010) define a dense phase as having a solid loading ratio greater than 15. Loading ratios less than this are called dilute phase. Most industrial pneumatic conveying systems operate in the dilute phase, including those of agricultural air seeders, thus, dilute phase pneumatic conveying was the focus of this literature review.

A consistent solids mass flow rate to all delivery points on the air drill (openers) through time is an important performance metric of modern air drill pneumatic conveying systems. Many manufacturers use a Type B pneumatic conveyance system (Allam & Wiens, 1982) with two stages: seed and/or fertilizer (generally referred to herein as product) is mechanically metered into individual *primary* air hoses/tubes. An example is shown in **Figure 1**. These meters are located on the air cart, which also includes the product storage tanks. Primary tubes are typically constructed of metal on the air cart, and then transition into flexible hose where the cart and air drill connect. Depending on the air cart manufacturer, a manual or semi-automated procedure is used to calibrate a relationship between metering roll rotations and product mass.

Figure 1. Primary meters controlling mass flow rate of solid product into primary distribution hoses.

Primary hoses convey the product to a secondary manifold that further divides the product and air streams into numerous secondary hoses; these secondary hoses terminate at the hoe openers of the air drill. The number of primary hoses varies, typically between 5 and 7. Secondary manifolds typically have between 6 and 12 secondary hose outlets. Secondary manifolds and hoses are shown in **Figure 2**.

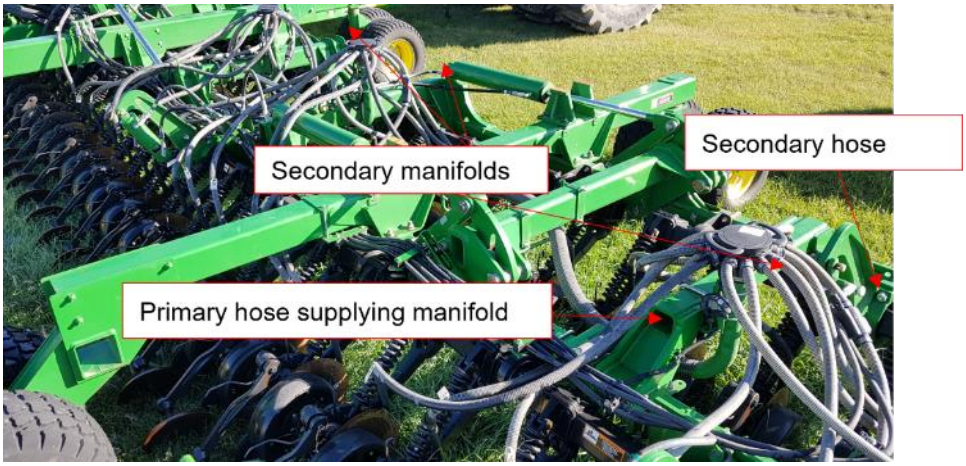

Figure 2. Secondary manifolds located on the air drill frame. The division of product and air occurs passively in the secondary manifold.

Many manufacturers use a steel, J-shaped tube to transition from the nominally horizontal flexible primary hose to the distributor body, which are commonly supplied from the underside. This J-tube is evident in **Figure 3**.

Figure 3. J-tube transitioning from nominally horizontal flexible secondary hose to the secondary distributor which is fed from the underside.

Modern features, such as sectional control, turn compensation, and variable rate application are achieved by individually varying the meters that feed product into the primary hoses, typically via an electronic control system. However, the division of product in the distributor into the secondary hoses is achieved only through the passive division of the air/product streams.

The source of air flow to the pneumatic conveying system is typically one centrifugal fan (typically hydraulically driven) located upstream of the metering system on the air cart. All primary hoses are connected via a common plenum to the centrifugal fan, shown in **Figure 4**.

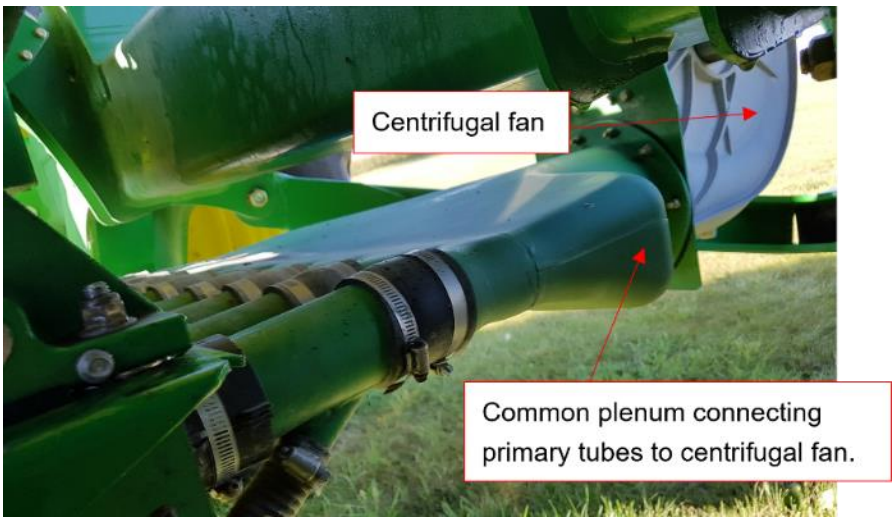

Figure 4. A centrifugal fan, the air flow source for the pneumatic conveying system, connected to primary tubes via a common plenum.

Air carts operate in an open-loop sense; that is, a feedback system is not present to confirm or maintain a constant solids mass flow rate in either the primary or secondary hoses. This has two major implications to the operator:

1. Consistency of the solids mass flow rates in the secondary hoses cannot be guaranteed.

2. An additional monitoring system is required to ensure that primary or secondary hoses have not plugged due to the accumulation of product.

To predict the solids mass flow rate in an air seeder line Hossain (2014) developed two semi-empirical mathematical models applicable to dilute phase horizontal pneumatic conveying. Measurement inputs to the models were pressure gradient and average air velocity. One model focused on the transient region 0.3 m to 0.9 m downstream of the product meters when wheat was being metered. The second model, applicable to any product, involves an on-machine parameter estimation procedure when the air drill is in use to correlate model parameters.

To further understand the flow conditions prior to plugging when conveying wheat, (Mittal, 2016) conducted extensive laboratory testing to develop the state diagram (a plot of pressure gradient versus air speed) for various solids mass flow rates of wheat conveyed through straight and bend sections of hose of similar diameter of typical primary hose. Distributor and secondary hose components were not part of the apparatus. For a given system configuration (hose length, bend radii, etc.), the pressure gradient increased with increased solids mass flow rate for a fixed air speed; a generic state diagram is shown in **Figure 5**.

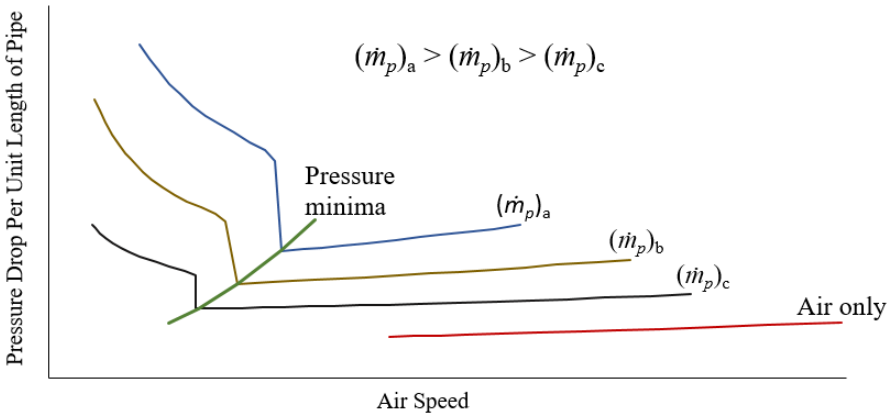

Figure 5. Generic state diagram plotting pressure drop against air speed for different solids mass flow rates. Reproduced with permission (Mittal, 2016).

As airspeed was decreased, pressure gradient decreased to a minimum value; below this minimum critical speed, the pressure gradient increased sharply. Near the critical speed, product saltation was observed: grain began to settle out of the air stream and bounce and roll along the bottom of the tube (Mittal, 2016). Hubert & Kalman (2003) compared several published analytical relationships between saltation velocity and solids loading ratio. The critical speed is typically viewed as the threshold of dense phase conveyance; plugging would eventually occur if the airspeed was reduced further. As the flow transitions to dense flow, pulsing of the product occurs (Keep, 2016) which results in an inconsistent solids mass flow rate and unsteady operation of the pneumatic conveying system. These are undesirable effects for the pneumatic conveying system of an air seeder as passive product division in secondary manifolds typically relays on the solids being properly suspended in the airflow.

Practically, operators typically set the fan speed to maintain the airspeed in primary hoses well above the minimum airspeed required to convey the product to decrease the risk of plugging. Susceptibility to damage from pneumatic conveying is dependent on seed type: Grieger (2018) found that germination of soybeans depended to some effect on conveyance airspeed, and it was strongly influence by seed moisture content. Chung (1969) reported measurable damage to yellow corn based on air speed and conveyance distance. In an assessment of two different system manufacturers, vigor reduction in canola from conveyance was estimated to be between 5% and 10% depending on the variety of canola and equipment manufacturer (Bjarnason, Stock, Hultgreen, & Wassermann, 2005).

In field trials, Yatskul, Lemière, & Cointault (2017) found that the orientation of the primary hoses upstream of the secondary manifold affected the coefficient of variation of the distributor. Further laboratory experiments on a distributor with 20 outlets highlighted performance trends under several operating scenarios when conveying wheat. When individual outlets of the distributor were closed, an increase in the solids mass flow rate occurred not in the outlets immediately adjacent the closed secondary outlet, but in the outlets further from the closure. An increase in static pressure at the plug face was noted, and seeds were observed to first move toward the plugged outlet, then be redirected by the airflow after bouncing off the outlet plug. Biased seed flow toward outlets not immediately beside the plugged outlet was theorized to be a result of the angular distance between outlets (dependent on design geometry).

The effect of secondary relative hose length was also tested. One secondary hose was adjusted to be longer or shorter than a standard set-up. Long hoses trended toward behaving like a blocked outlet. The solids mass flow rate of a shorter secondary hose was higher than the standard length hoses. If an acceptable CV of 5% is assumed, the recommended relative hose length was between 0.8 and 2.5 of the standard hose length (Yatskul, Lemiere, & Cointault, 2017). Only one secondary hose (of 20) was modified in the experiment.

The geometry of the vertical pipe leading to the distributor affected the distribution uniformity. The vertical orientation and the length of the pipe were investigated. The distributor was rotated about the axis of the primary hose. The CV of distributors with smooth vertical steel pipes was more negatively impacted than distributors with corrugated/dimpled vertical pipes. Distributors with shorter tubes also had lower uniformity, with seed flow greater in the outlets that aligned with the primary hose. The authors recommended J-tube heights greater than 1.2 m (Yatskul, Lemiere, & Cointault, 2017). The introduction of a cone to the center of the underside of the distributor access lid was found to decrease the distribution uniformity. Considering the sensitivity to vertical tube height, the authors highlighted the complexity of collisions in the elbow that transitions from the horizontal primary hose to the manifold tube. Kinetic equations were presented, but this single-kernel model was not verified as part of the experimental procedure.

Kumar and Durairaj (2000) presented an experimental investigation of the impact of distributor geometry on the performance of air drills. Three different distributor geometries were considered

along with the input air velocity (four levels) and seed feed rates (four levels). They highlighted a significant impact of the manifold geometry on the air velocity at the outlets of the distributor. Two important observations made by Kumar and Durairaj were (1) one of the distributors exhibited threshold values of seed feed rate and input air velocity under which uniformity of seed distribution was poor, and (2) after the threshold value, the dependency between uniformity and seed feed rate remained strong. This was a very good study that provided statistically analyzed experimental results. It, however, did not consider factors downstream of the distributor (primarily tube length and routing) nor the operational implications at the system level.

4.2 Simulation of Pneumatic Conveying Systems

The complexity of pneumatically conveying grain is evident from the experimental research presented. Product type, solids mass flow rate, conveying airspeed, and details of the system geometry are but some of the factors that affect that state of the system and subsequently the distribution uniformity. The ability to experimentally quantify system performance under so many conditions is daunting if not futile. Several researchers have developed numerical models of various aspects of the pneumatic conveying systems of air seeders to further understand performance features.

Bourges et al. (2008) performed a computational fluid dynamics (CFD) analysis of the results presented by (Kumar & Durairaj, 2000). Bourges & Medina (2013) numerically studied a commercial secondary manifold using a weak coupling approach where the solid phase (product) is affected by the fluid phase, but the particles have no effect on the air velocity. The Langrangian-Eulerian method was used to track the discrete solid particles in the simulation. Their results matched anecdotal evidence on the irregular distribution out of the distributor. The authors suggested the need to include the coefficient of restitution of the seeds to represent seed collisions more accurately. Here again, the authors did not elaborate on the implications of the observed behaviours on the performance of the overall system.

Cousins and Noble (2017) developed a 1-D CFD model intended for real-time control applications on an air seeder. A two-fluid (Eulerian-Eulerian) approach was used to model a straight section of air seeder primary hose. Fluid pressure predictions were found to be in good agreement with experimental data; however, solids velocities were not as accurately predicted. Improvements to model features, such as drag force estimation, were suggested. Because of the 1-D nature, particle-wall and particle-particle collisions were not represented explicitly; axial momentum loss was represented parametrically from the approach of (Eskin, Leonenko, & Vinogradov, 2007), which includes the coefficient of restitution. Considering the interest in understanding impacts between the seed and the pneumatic system geometry, a two-fluid approach is not appropriate for this project.

Bourges and Medina (2015) later investigated three different configurations of the outlets of a distributor and included the coefficient of restitution when modeling particle impacts. They

observed non-uniform distribution but did not offer analysis of the observed flow patterns. In subsequent work (Bourges, Eliach, & Medina, 2017), CFD simulations of the distributor with soybeans and amaranth particles were presented. The realizable k-ε turbulence model was used, along with sphere-shaped particles of uniform size for a given seed type. Elastic particle-boundary collisions were represented. Solids mass flow rates at the distributor outlets were not consistent: the uniformity of soybeans was lower than the amaranth, and the patterns were not consistent with air flow patterns. The lower outlet variation of amaranth was attributed to it having a lower Stokes number than soybeans. System-level observations were not provided.

In a white-paper from Bayati & Johnston (2017), two modeling approaches were presented, with a focus on variance of the solids mass flow rate in secondary hoses through time. Both wheat and soybeans were modeled: one-way coupling was used in the wheat simulations, due to its low momentum coupling factor; soybean-air interactions were modeled using two-way coupling where the particles and air affect each other as the momentum coupling factor was an order of magnitude larger than that of wheat. The standard k-ε turbulence model was used, along with the Langrangian method to track particle motion within an Eulerian representation of the fluid. The larger soybean particles tended to cluster (high solids mass flow rate variance through time at the manifold outlets). Both particle types tended to stagnate in the manifold until adequate pressure was developed to carry the seeds down the secondary hoses.
Ebrahimi (2014) provided a road map for developing and experimentally validating a CFD-DEM pneumatic conveying model using both spherical glass beads (0.9 mm, 1.5 mm, and 2.0 mm mean diameters) and cylindrical polyamide6 particles (1 mm x 1.5 mm). Particle and air velocity were measured using laser Doppler anemometry. Measured velocity profiles through both vertical and horizontal cross sections at multiple solids loading ratios and at multiple distances downstream of the injection point were reported for both the carrier fluid (air) and the particles in the experiments involving both particle types. Similarly, the turbulence intensity profiles of the carrier fluid from the experiments were reported.

Additionally, Ebrahimi (2014) evaluated the influence of the Magnus lift force on spherical particles in the coupled CFD-DEM model by comparing its contribution compared to gravitational and drag forces as well as considering the number of particles that were carried in the upper portion of the pipeline cross-section (i.e., the probability distribution of the vertical position of seeds; additional experimental results of this quantity for conveying wheat are provided in Keep (2016). The Magnus lift force model was included in subsequent simulations (Ebrahimi, 2014). For cylindrical particles, the effect of the Ganser (1993), and Haider and Levenspiel (1989) drag models were investigated. Both of these models are available as particle body forces in EDEM (Altair Engineering Inc., 2021) discrete element method software, which will be used as the DEM simulation engine for this project.

Boac et al. (2010) compiled a comprehensive list of physical parameters for a variety of seed types from the literature, including canola and wheat; however, the coefficient of restitution for boundary collisions was not reported.

5. FULL-SCALE AIR DRILL TESTING

Through February and March of 2021, PAMI rented a John Deere 1870 double-shoot hoe drill (56-ft width) paired with a 1910 air cart (550 bushel) to conduct experiments on a full-scale machine. Along with seed mass distribution uniformity, air velocity and static pressure were measured at various locations in the pneumatic conveying system. Seed mass measurements provide a direct measurement of the uniformity of seed distribution across the whole air drill. Airflow measurements were collected to characterize the physical performance of the conveying system to support the development of computational fluid dynamics models.

The air drill and commodity cart are pictured in **Figure 6**. In general, a cart with individually metered primary hoses was chosen due to the common use of that metering configuration across western Canada. The particular brand and model were selected based on dealer rental unit availability and cost at the time of testing.

(a) (b)

Figure 6. The John Deere 1870 hoe air drill (a), and 1910 air cart (b) used for testing at PAMI in Humboldt, Saskatchewan.

Materials and methods are discussed in **Section 4.1**; data analysis is discussed in **Section 4.2**; results are presented and discussed in **Section 4.3**.

5.1 Materials and Methods

The John Deere 1870 double shoot drill (56-ft width) with hoe openers and John Deere 1910 air cart (550 bushel) used for testing remained indoors at PAMI's test facilities throughout the duration of the test period. A "double-shoot" configuration of the machine enabled separate metering, conveyance, secondary distribution, and application of (typically) seed and fertilizer streams, via separate, nearly duplicated, pneumatic conveying systems. However, the air cart had a single centrifugal fan. The machine was configured with 12 primary runs in total: six for seed distribution and six for fertilizer. The fan, plenum, and start of the primary tubes on the air cart are visible in **Figure 7**.

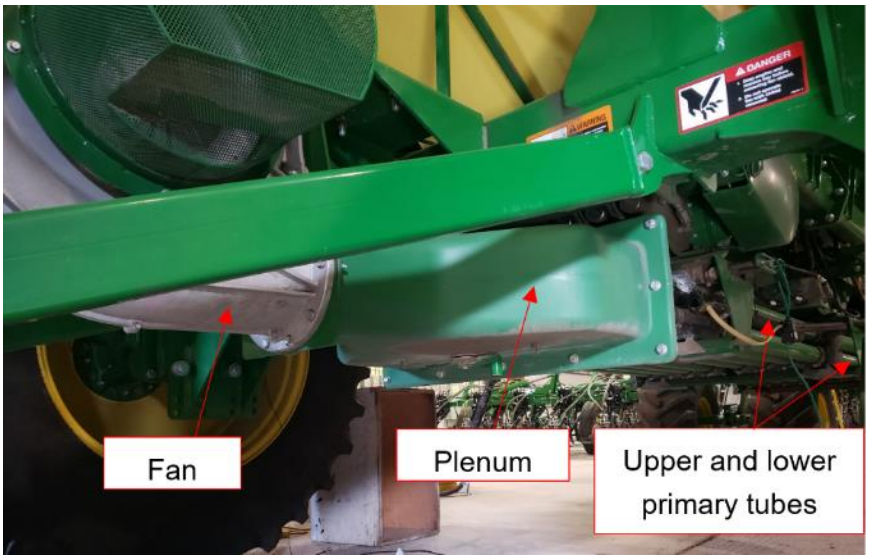

Figure 7. The fan, plenum, and upper and lower sets of primary tubes, from left to right in the image, visible at the back of the air cart.

Pneumatic system parameters are summarized in **Table 1**. The primary hoses and distributor towers were numbered from left to right as viewed from behind the drill looking forward.

Table 1. John Deere 1870 air drill hose layout and length data (± 0.01 m). Primary hose length was measured from the coupler plate between the air cart and drill.

Distributor Number	Secondary Outlet count	Primary Hose Length (m)	Secondary Hose Length (m)		
			Average	Minimum	Maximum
1	10	9.25	2.27	1.68	2.67
2	9	6.40	2.54	1.45	3.96
3	10	2.08	2.32	1.73	2.92
4	9	2.36	2.47	1.60	3.51
5	9	6.58	2.68	1.78	4.52
6	9	9.37	2.20	1.63	2.74

Per the operator's manual, the adjustable baffle in the air cart fan plenum (**Figure 7**) was adjusted to its extreme position for single-shoot operation; the intent of this adjustment was to direct as much air as possible down just one set of primary lines. The fan was powered by a hydraulic power pack; as electrical power was supplied to the machine, the cab monitor system was used to determine the speed of the fan.

The 1910 air cart has three separate product tanks; only the front tank was filled during this testing. Meter rollers were located at the bottom of each tank to introduce product (seed or fertilizer) into the primary tubes; product can be introduced into either the top or bottom set of primary tubes. A single fluted roller was used in each meter to dose product into the primary hoses; rollers are specified by the manufacturer based on product size and metering rates. The roller used for canola is shown in **Figure 8**, with six distinct segments to meter product into six primary hose routes. The fraction of open area in each of the six segments of the roller was proportional to the number of hoe openers (secondary hoses) sourced by each segment.

Figure 8. The meter roller used for canola testing, as specified by the manufacturer.

A square-wave signal generator was used to emulate the speed signal received by the meter roller motor in order to conduct stationary testing. Tests were conducted based on the air drill traveling at 8.0 km/h while applying 5.60 kg/ha, the often defaulted-to rate of “5 lb/ac at 5 miles per hour.” InVigor® L233P treated canola was used for all pneumatic conveying tests.

Downstream of the meters, the primary tubes were inclined upwards to pass over the front axle of the air cart. This up-sloped portion of the tubes are visible at the right edge of **Figure 6 (b)**. The primary tubes then transition to flexible hose material until reaching each steel distributor tower tube. The routing of the primary hoses between the air cart and drill frame are shown in **Figure 9**. Couplers to separate the cart and drill are also annotated in the figure.

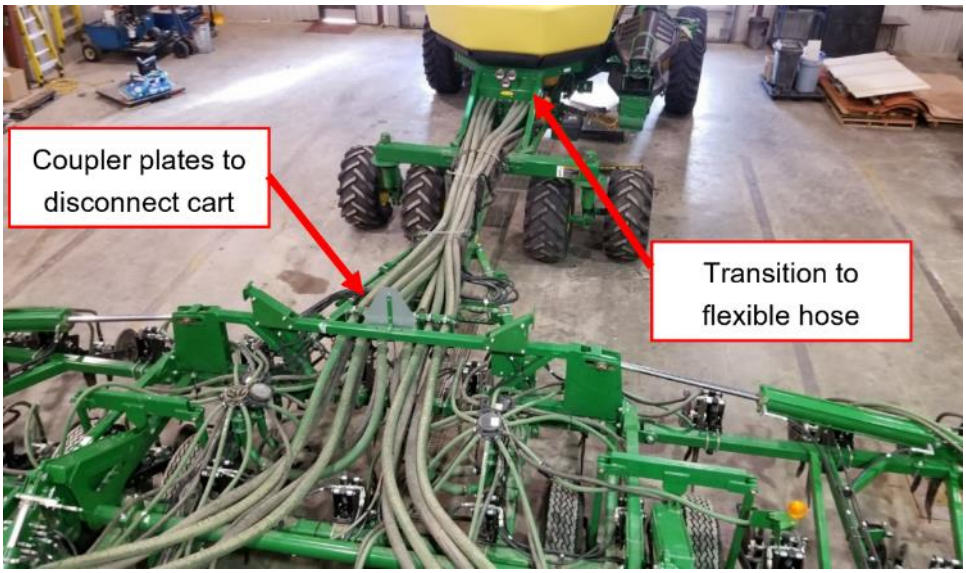

Figure 9. The routing of the primary hoses downstream of the steel tubes on the air cart.

The hose routings on the left wing of the air drill are visible in **Figure 10**, including the three distributor towers for each product type on the left half of the machine.

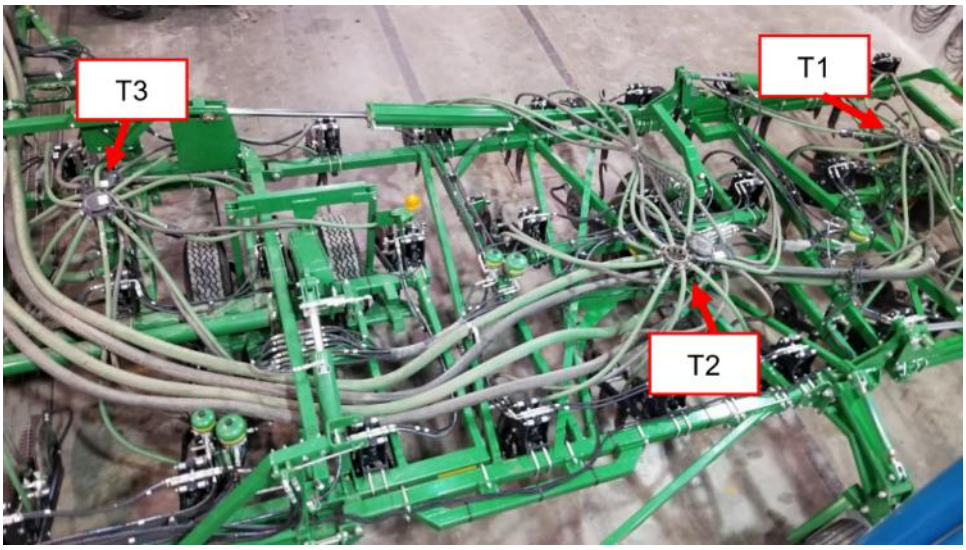

Figure 10. Hose routes are visible on the left half of the drill (looking backwards), along with the three distributor towers for each product stream for that half of the drill. The left outer edge of the air drill is visible at the right of the image.

The primary hose routes were fairly symmetrical across the width of the drill (i.e., the geometry of primary hose 1 and 6, 2 and 5, and 3 and 4 were fairly similar); however, the hose geometry between these three pairs different greatly. Upstream of distributors 1 and 6, hoses had a sweeping horizontal bend followed by a vertical drop leading up to the distributor, as seen in **Figure 10**.

Runs 2 and 5 had a much straighter approach the distributor, as seen in **Figure 11**.

Figure 11. The primary hose leading up to distributor 2.

Runs 3 and 4 had the most severe curvature upstream of the distributor due to the short distance where the distributors were placed and where the primary hoses entered the drill frame from the air cart. Distributor 3 is shown in **Figure 12**.

Figure 12. The primary hose geometry leading to distributor 3. Distributor 4 had similar geometry.

Finally, secondary hoses were routed from the distributor towers to each row unit. In the single-shoot configuration the front hoe opener was supplied canola (green hose in **Figure 13**).

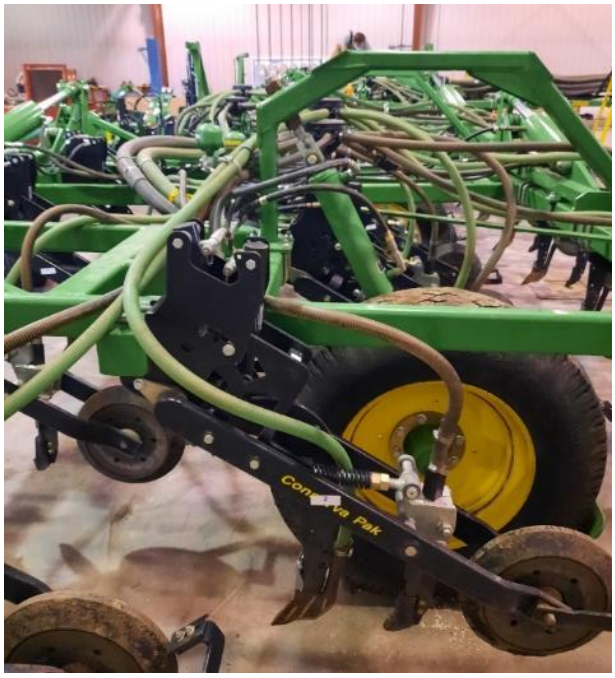

Figure 13. One of 56 row units on the air drill. In the single-shoot configuration, the front green hose supplied seed to the hoe opener.

To collect the canola seeds during the distribution testing, mesh bags were fastened around each seed opener as shown in **Figure 14**. Bags were numbered to relate the deposited seed amounts to specific openers.

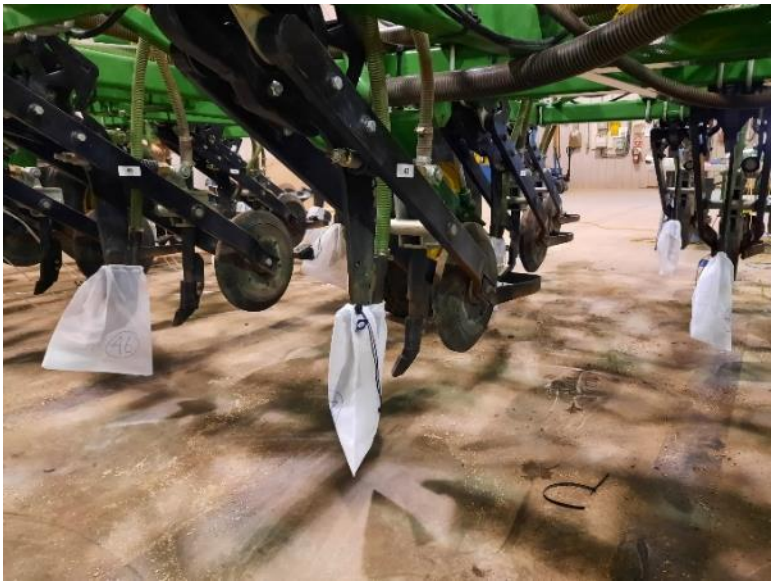

Figure 14. Numbered mesh bags fastened to each row unit to capture the canola distribution.

The bags were weighed using a precision balance (Mettler Toledo MS6002S, linearity = 0.02 g, repeatability 0.01 g).

To measure the air velocity and static pressure within the hoses of the pneumatic conveying system, pitot-static tubes were installed by piercing the hoses at selected locations on the air cart and drill and supporting the tube with a bracket that clamped onto the hose to maintain the position of the pitot tube within the pneumatic system hose. Instrumentation details are given in **Table 2**.

Table 2. Instrumentation details.

Instrument	Manufacturer	Model	Range	Accuracy (% F.S.*)
Pitot static tube	Dwyer	Series 160 – 1/8" diameter	400-8000 ft per min	5.0
Differential pressure transducer	Dwyer	648C-7	0-10 inches H20	0.4
Data acquisition	Somat	EBRG-350-B-2	0-400 mV to ± 10V	0.10

*F.S. – Full scale range

Broadly, the measurement of air velocity and static pressure within the pneumatic conveying system was separated in "air only" and "air and seed" measurements, as summarized in **Table 3**.

Table 3. Instrumentation configurations and operating states during data collection efforts.

Instrumentation Location	Operating State
Six primary hoses at three streamwise locations	Air only
Subset of primary/secondary hoses	Air only and then with seed

Due to limited instrumentation (20 pitot-static tubes) and the cost of canola seed (seed could not be reused, as vigour was tested after being metered through the system), air velocity and static pressure were first measured in all six primary hoses at three streamwise locations without injecting canola (“air only”). Pitot static tubes were installed immediately downstream of the transition to flexible hose at the air cart (**Figure 15 (a)**), immediately upstream of the coupler between the air cart and drill (**Figure 15 (b)**), and upstream of each distributor (**Figure 16**).

(a) (b)

Figure 15. Pitot-static tubes in all six primary hoses installed immediately downstream of the tank (a), and immediately upstream of the couplers (b).

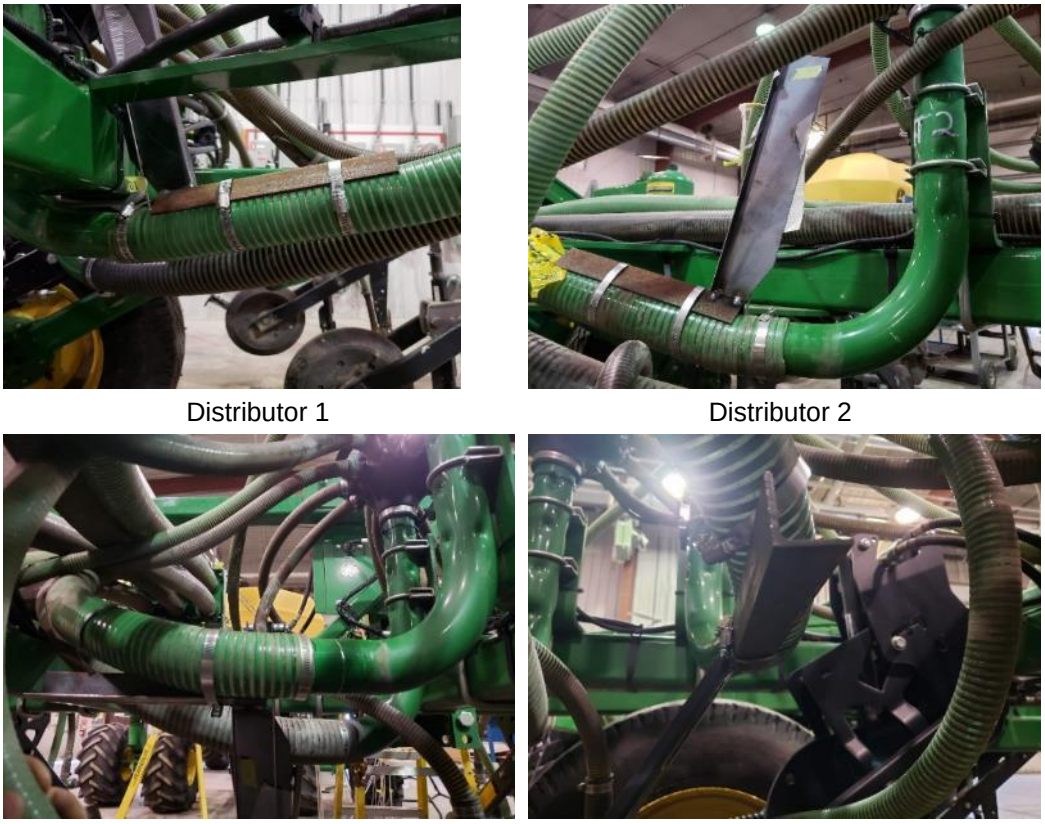

Distributor 1 Distributor 2

Distributor 3 Distributor 4

Figure 16. Pitot static tube installation locations upstream of distributors 1 to 6.

Distributor 5

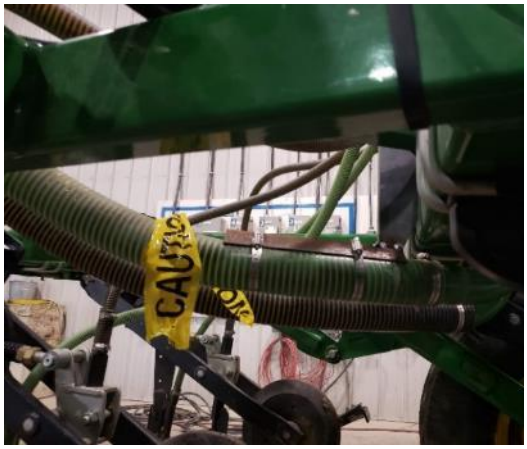

Distributor 6

Figure 16 (continued). Pitot static tube installation locations upstream of distributors 1 to 6.

The pitot tubes were installed to keep the tip of the pitot tube in the center of the tube as best as possible, to read the maximum air velocity in the hose (under the assumption of fully developed flow). Alignment was challenging at distributors 3 and 4 due to the curvature of the primary hose.

When canola was being conveyed, a second layout of pitot tubes was employed where instrumentation was installed in only a subset of primary hoses, along with some secondary hoses. Pitot tubes at the tank remained installed in primary hoses 4 and 6 to enable comparison back to the air-only data. The remaining 18 pitot-static tubes were installed in the secondary hoses of distributors 4 and 6 just upstream of the hoe opener boot. An example of the installation at the opener is shown in **Figure 17**.

Figure 17. A pitot-static tube installed at a row unit downstream of distributor 4 or 6.

With only ten pressure transducers available, measurements from only one set of primary/distributor pitot-static tubes were recorded during each replication. Replication details are summarized in **Table 4** below. Note that while the airflow measurements were only taken on one distributor per replication, seed was collected from all openers during all replications.

Table 4. Operating and data collection details for trials with seed.

Fan Speed (rpm)	Replication Number	Distributor for Air Measurement Data
2200	1	4
	2	6
	3	6
2800	1	6
	2	4
	3	4
3400	1	4
	2	6
	3	6

The nature of differential pressure measurement and pitot-static tube function was exploited to measure both the velocity and static pressure at the various instrumentation locations. By their nature, pitot-static tubes exploit the difference between velocity pressure and static pressure to calculate a fluid velocity. By disconnecting the velocity pressure port from the pressure transducer, the static pressure at the pitot tube location was measured (asynchronous to the velocity measurements). Specifically, the test procedure for each replication was as follows:

1. Installed the appropriate fabric bag onto each opener.
2. Turned the air cart fan on and warm up let the hydraulic system warm up for approximately 30 seconds.
3. Measured air-only velocity pressure for >60 s.
4. Turned on seed meters for ~212 s.
    a) Measured velocity pressure for 90 s.
    b) Changed instrument tubes to static pressure.
    c) Measured static pressure for 90 s.
    d) Turned seed off.
5. Measured air-only static pressure data collection >60 s.
6. Shut off fan.
7. Collected the seed bags and weigh them. Bag tare weights were recorded prior to the start of testing.

Based on the simulated test conditions (5 lb/ac seeding rate at 5 mph), the theoretical seed mass delivered to each opener over the test period was 80.6 g.

The arrangement of pressure transducers is shown in **Figure 18**.

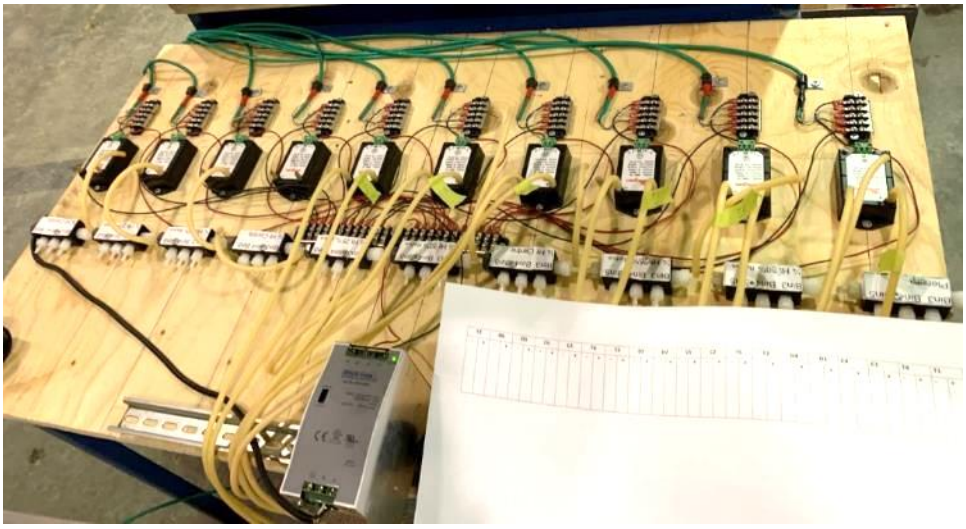

Figure 18. The pressure transducers used for measuring velocity and static pressure with the pitot-static tubes installed on the air drill.

5.2 Data Analysis

Seed samples from each trial were combined and mixed with samples from the same distributor after mass measurements were collected from each replication. Additional control samples were collected prior to testing the air drill. A sample was taken from this “per distributor per replication” seed mixture and sent to Discovery Seed Labs for germination and vigour analysis after air drill testing was completed.

The seed mass collected from each opener was weighed and recorded. To correct for possible runtime differences (the seed meter was stopped manually, and delays were noted on some trials), the sample mass was normalized by the total mass of seed collected during each replication. Multiple replications enabled the calculation of variance between trials per opener, subsequently referred to as coefficient of variance 1 (CV1); CV was defined as the ratio of the variance divided by the mean of the samples of interest. Variance between openers (not grouped by distributor) was calculated for each replication, referred to as CV2. Finally, the variance within each distributor, deemed CV3, was calculated.

Air velocity was measured as velocity pressure (P_v) and converted to a linear speed (units of m/s) by **Eq. [1]**:

$$V = 5.569\sqrt{\frac{P_v}{\rho}}\,. \qquad \textbf{[1]}$$

where ρ is the density of the air. Static pressure was measured directly by disconnecting the total pressure sensing tube.

The contributions of the HQP involved in the project, M.Sc. student Sarita Victoria Casas Urrunaga, are acknowledged through her summarization of this testing activity, and initial analysis of the germination, seed distribution, and airflow measurements.

5.3 Results and Discussion

Once the data were collected, three main aspects were considered for analysis: the germination and vigour results to quantity the effect of seed damage caused by metering and pneumatic conveying at the three different fan speeds, the consistency of seed distribution across the air drill, and finally the airflow within the pneumatic conveying system.

During documentation and clean up after testing, it was noticed a piece of debris was caught in distributor 3, partially blocking secondary hoses in position 1 and 2 of the distributor. **Figure 19** shows the debris as it was found when the distributor lid was removed.

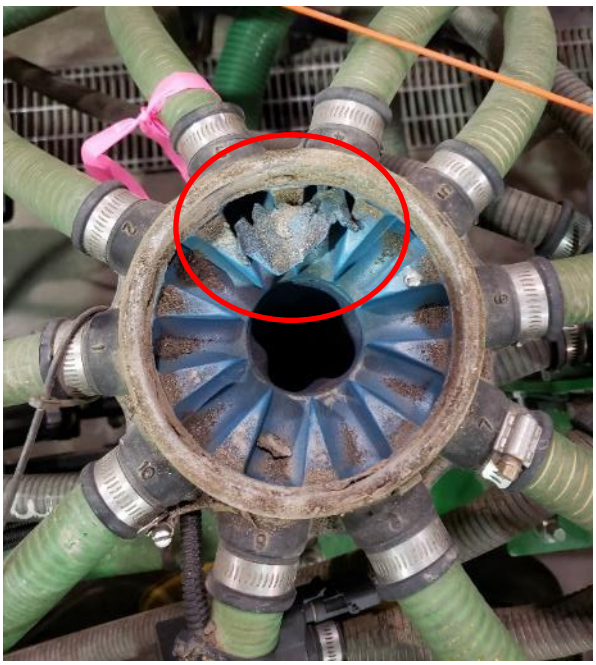

Figure 19. Debris found in distributor 3 at the conclusion of testing, partially blocking outlets 1 and 2.

Seed mass data from these openers were removed from the data, leaving seed mass measurements from 54 openers for general analysis.

5.3.1 Germination Results

A one-way analysis of variance (ANOVA) of the germination results was conducted with R (R Core Team, 2021) using a linear model with fan speed and distributor numbers as factors. No significant difference was found between the group means. From this result, it was concluded that the germination of this canola variety, under the given test conditions, was not affected by the pneumatic conveying experiments.

5.3.2 Consistency of Seed Distribution

Statistics for CV1 (across 54 openers) for the three fans speeds are reported in **Table 5**.

Table 5. Statistics across 54 openers for CV1 results across the three fan speeds during testing.

Fan Speed (RPM)	CV1 (%)		
	Average	Minimum	Maximum
2200	0.71	0.03	1.41
2800	0.52	0.06	1.25
3400	0.58	0.11	1.68

Overall, the within-opener, run-to-run variation was very small across the air drill, no strong trend was evident in relation to fan speed. Considering the theoretical seed mass delivered to each opener over the 212 s duration of each replication, the average CV1 values represent a variation in seed mass ranging between 0.42 - 0.56 g. Note that the removal of the debris-blocked measurements had minimal effect on the average value of CV1 and did not change the reported values of minimum or maximum CV1.

Extending this variation to field operations, this translates to a difference in the number of seeds delivered by a given opener, from one duration to the next, ranging between 89 to 119 seeds over the 473.8 m of simulated linear distance travelled during the test. This is based on the thousand seed weight (4.7 g) reported for the canola used during the trial.

Values for CV2 are plotted in **Figure 20**.

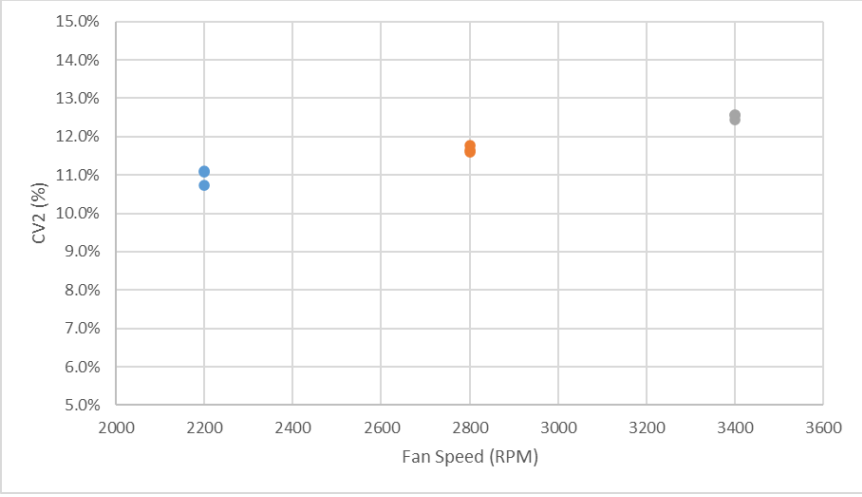

Figure 20. CV2 of each replication at the three fan speeds tests.

The trend of increased CV2 with greater fan speed is evident, indicating that the variation between row units across the whole air drill was proportional to fan speed. A one-way analysis of variance (ANOVA) was conducted using R (R Core Team, 2021), which indicated significant differences between the group means, at a significance level of 0.05. A further Tukey Honest

Significant Differences test was conducted, which indicated that the three groups were all significantly different from each other.

It is noted that the lowest fan speed (2,200 RPM) was the fan speed suggested by the operator's manual for the seed type and mass flow rate under consideration. Therefore, it was concluded that, for this air cart/drill combination under the given operating conditions, increasing the fan speed beyond what was suggested by the operator's manual would needlessly decreased distribution uniformity while likely increasing hydraulic power consumption.

Within-distributor variation, CV3, is plotted in **Figure 21** for all distributors, including #3; its outsized variation is evident in comparison to the other distributors. Unless specifically noted, distributor #3 is not included in the subsequent analysis.

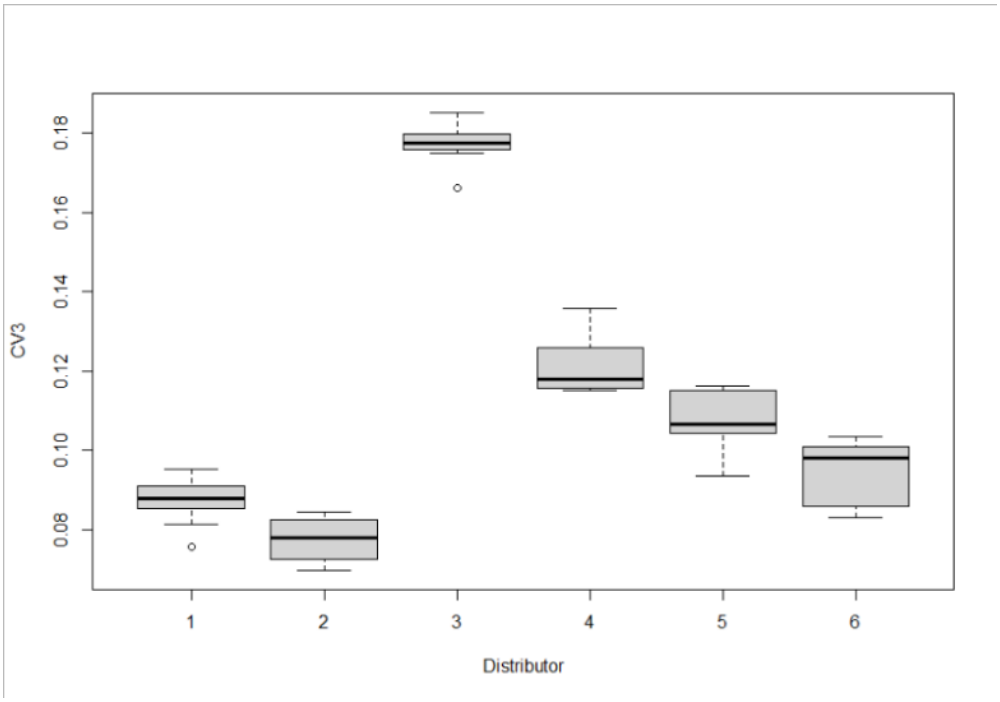

Figure 21. A box-whisker plot of the within-distributor variation, CV3, of all six distributors averaged across the three fan speeds. Each box-whisker bar is based on nine data points with circles indicating outlier values.

The average CV3 ranged between a minimum of 7.7% for distributor 2 and maximum of 12.1% for distributor 4 (excluding 3). Values for the two outermost distributors (1 and 6) were similar, but the difference between distributors 2 and 5 was more extreme. The CV3 value of distributor 4 was the greatest of those considered in the remaining analysis.

As fan speed was also varied during the experiments, a one-way ANOVA was performed including the distributor position and fan speed as categorical variables in a linear model with an interaction term. Both individual factors were found to be statistically significant, but the interaction term was not. Increased fan speed resulted in a proportional increase in distribution

variability. An additional Tukey HSD analysis indicated that the means of all RPM treatments and all distributor treatments were significantly different.

The mean CV3 values for the three different fan speeds are shown in **Table 6**, along with their percent difference from the lowest speed.

Table 6. Average CV3 values for the fans speeds tests.

Fan Speed (RPM)	Average CV3 (-)	%-difference from 2,200 RPM
2,200	0.0904	-
2,800	0.0975	7.85
3,400	0.104	15.0

These results further strengthen the recommendation that, for the conditions test, operating with a fan speed greater than that suggested by the operator's manual is detrimental to the consistency of seed distribution across the air drill.

Actual seed mass distribution values were further analyzed with the additional consideration of secondary hose length, and the relative position of the secondary hose within each distributor. Secondary position 1 was taken to be the secondary hose inline with, or immediately counterclockwise (as viewed from above) to, the inlet of the distributor elbow. Numbering proceeded clockwise from that location, such that the primary hose approached the distributor inline with secondary hose 1, or between hose 1 and 2.

To avoid creating a model with nested factors due to the difference in the number of secondary outlets in distributors 1 (10 outlets) versus the nine outlets of all other distributors under consideration (3 excluded), and the data imbalance that would result, only distributors 2 and 4 through 6 were considered. A linear model including the factors fan speed, distributor number, and secondary position, secondary hose length, and their interaction, was developed for the response variable of normalized seed mass per opener. A statistically significant model was fit, with $R^2_{adjusted} = 0.821$, where distributor number, and secondary position, secondary hose length, and their interaction were statistically significant, but fan speed was expectedly not significant. Removal of fan speed from the model had no further impact on the significance of other factors.

Several notable insights were gleaned from the results of this analysis:

- Secondary hose length was negatively correlated with the seed mass collected at the opener; that is, longer secondary hoses received less seed. This suggested an influence of secondary hose length on the dividing characteristics of a distributor. The working hypothesis, in line with Yatskul, Lemiere, & Cointault (2017), was that longer secondary hoses presented a greater back-pressure at the distributor resulting in less airflow passing through longer secondary hoses.
- The distribution of seed mass was influenced by the angular position of the secondary outlet in the distributor. This suggested a structural inconsistency in the division of seed among the

distributor outlets. The additional significance of the interaction between secondary hose length and position suggested that some angular positions were more sensitive to the hypothesized backpressure differences (due to hose length) than other locations.

- The factor for the distributor number should be interpreted as a variable that reflects the bulk differences between primary hoses, the most notable difference being the geometric routing of the primary hose upstream of the distributor elbow and vertical tube.

The distribution of seed as a function of the secondary outlet position within distributors 2, 4, 5, and 6 are shown in **Figure 22**. Note that the nominal mass fraction for 1 of the 56 openers on the air drill is 0.0178 (i.e., 1/56).

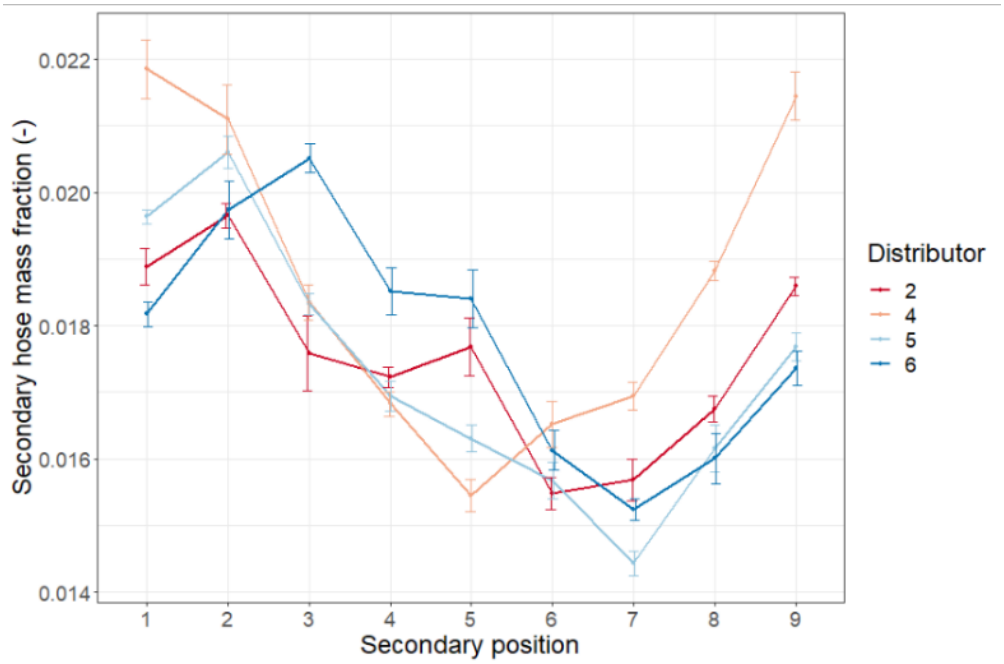

Figure 22. Seed mass fraction as a function of the secondary hose outlet position (1 to 9) for each distributor, across all three fan speeds. The error bars indicate 1 standard deviation.

A similar distribution pattern occurred in the four distributors shown in **Figure 22**. The greatest amount of seed was typically distributed through secondary position 1 and its neighbours (2 and 9). The least amount of seed was distributed through the secondary outlets diametrically opposite of position 1 (nominally position 5), although bias towards positions 6 and 7 is evident in **Figure 22**.

Finally, when seed mass (normalized by the total mass per distributor) is plotted against secondary hose length (**Figure 23**), the trend of more seed being distributed to shorter hoses is also evident. Hoses shorter than approximately 2.5 m tended to receive a greater portion of seed than hoses longer than 2.5 m.

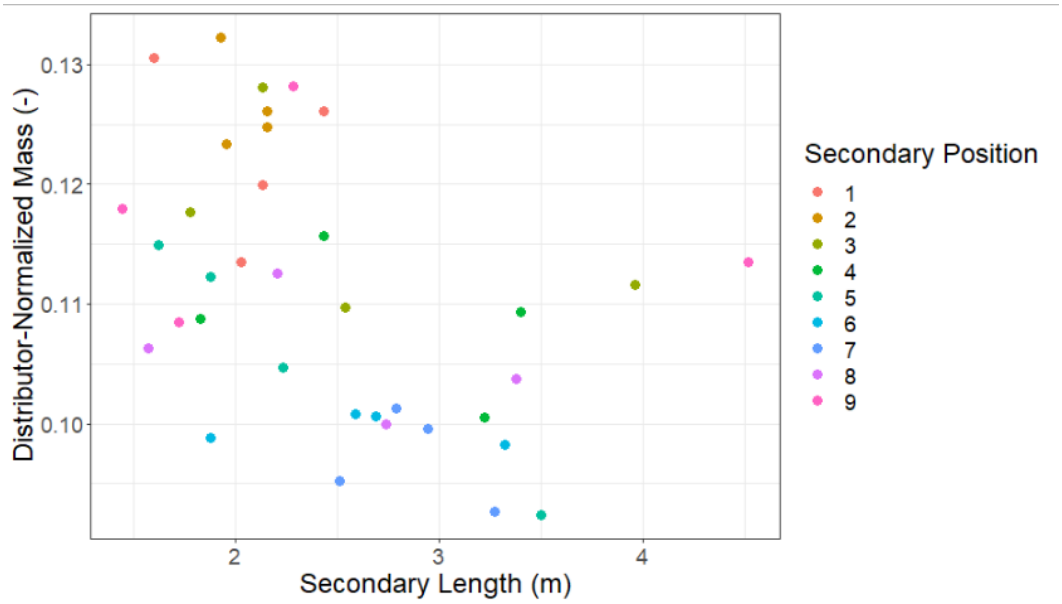

Figure 23. Average mass distribution per secondary hose (normalized by the total mass per distributor) as a function of secondary hose length, with color based on the secondary hose position.

5.3.3 Airflow Measurements

Finally, the air velocity and static pressure measurements collected from the various arrangements of pitot-static tubes were analyzed. Air-only results are presented first, followed by a discussion of the effect of the presence of canola seeds

The average static pressure values at the tank (T), coupler (C), and distributor (D) measurement locations are plotted versus the three fan speeds in **Figure 24** to **Figure 26**.

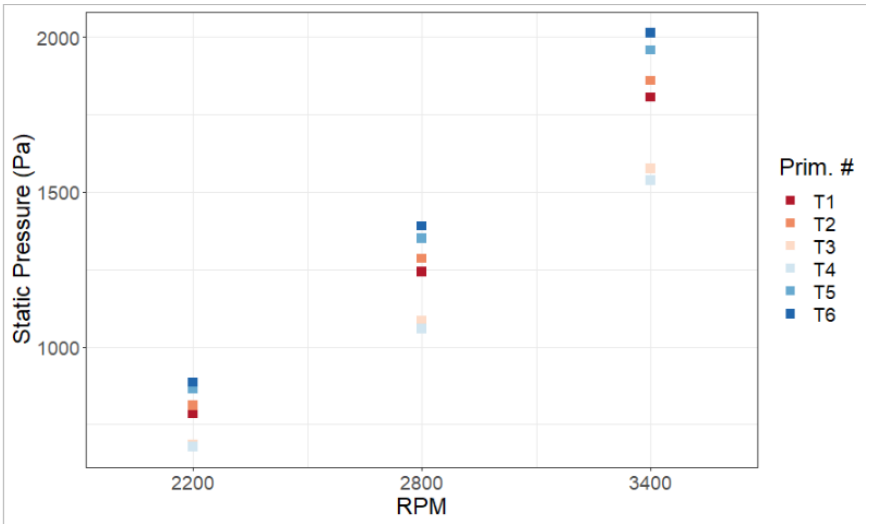

Figure 24. Average static pressure values for each primary hose measured at the tank location.

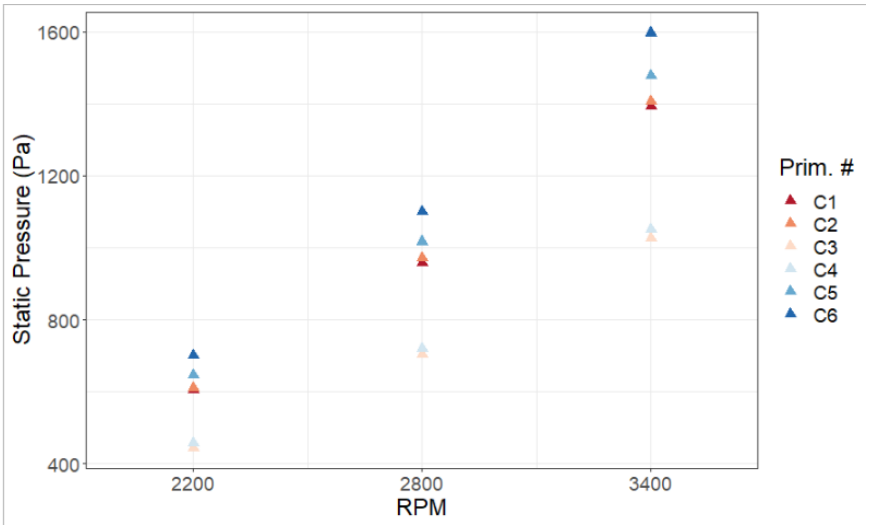

Figure 25. Average static pressure values for each primary hose measured at the coupler location.

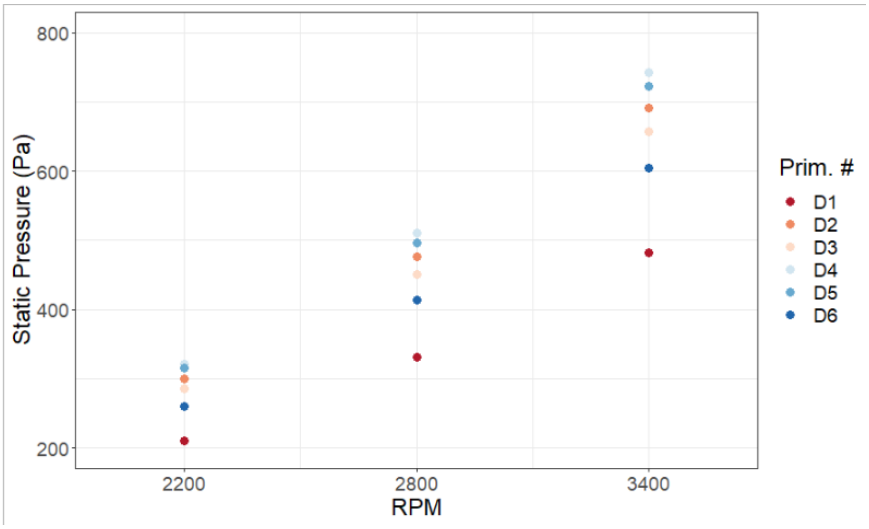

Figure 26. Average static pressure values for each primary hose measured at the distributor location.

Static pressure results were largely in line with expectations; however, stronger symmetry was expected between primary hoses 1 and 6, and primary hoses 2 and 5 at the tank and coupler locations. Line length effects were particularly evident in the relatively low-pressure readings at T3 and T4, and C3 and C4. As all primary hoses are “coupled” via the common plenum at the fan, hoses that present a lower resistance should see increased airflow through them, all other factors held equal.

Direct effects of primary hose length should not be discernable in the static pressure measurements at the distributor location (Figure 26), as static pressure represents the effort required to move the air through the system downstream of the measurement location (i.e., the J-tube and the distributor head itself, as well as the secondary hoses). However, the curvature of the primary hose in the vicinity upstream of the distributor measurement location may contribute to the static pressure measurements. The total length of secondary hose connected to each distributor is shown in **Table 7**.

The measured air speeds in the primary hoses, shown in **Figure 27,** provide as much characterization of the differences in air velocity in the primary hoses as they do commentary on the variation of airspeed across the diameter of the primary and the sensitivity of pitot tube placement.

Table 7. Total secondary hose length connected to each distributor tower.

Distributor No.	Total Secondary Length (m)
1	22.68
2	22.83
3	22.58
4	22.20
5	24.08
6	19.76

Some correlation between total hose length and the relative magnitude of static pressure measurements at the distributors was plausible, particularly for the maximum and minimum total lengths, distributors 5 and 6, respectively. Some interaction between the sharp bends upstream of distributors 3 and 4 and the relatively high static pressure measurements were suspected.

The measured air speeds in the primary hoses, shown in **Figure 27**, provide as much characterization of the differences in air velocity in the primary hoses as they do commentary on the variation of airspeed across the diameter of the primary and the sensitivity of pitot tube placement.

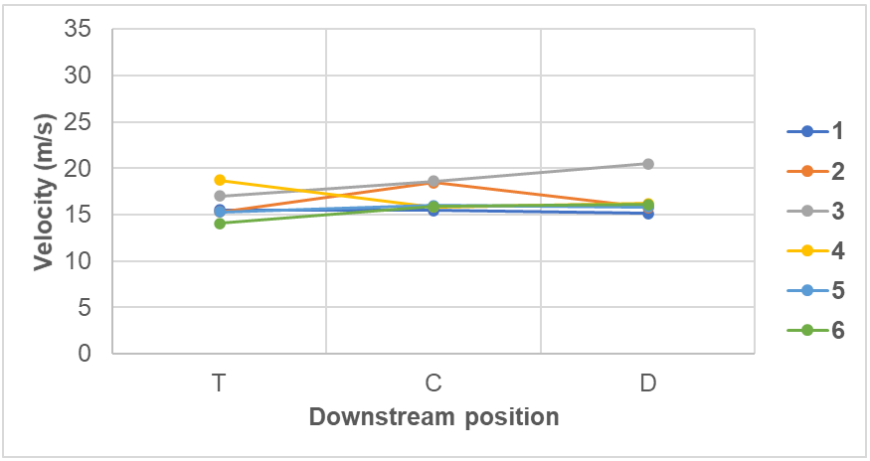

(a)

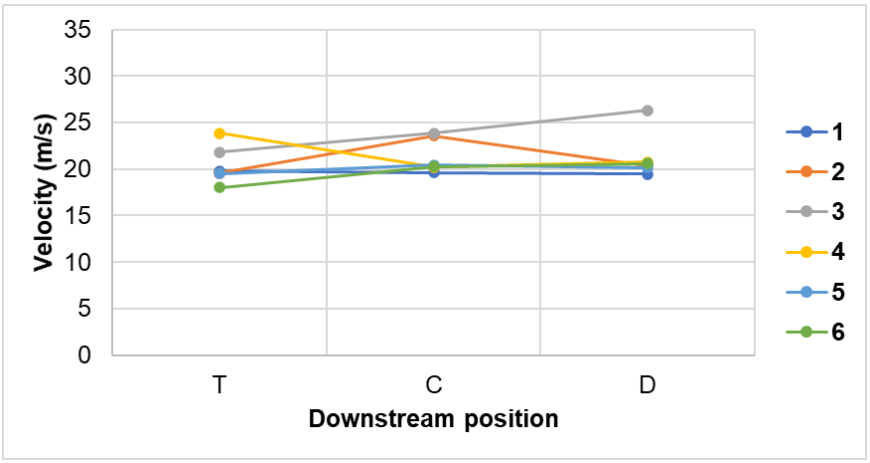

(b)

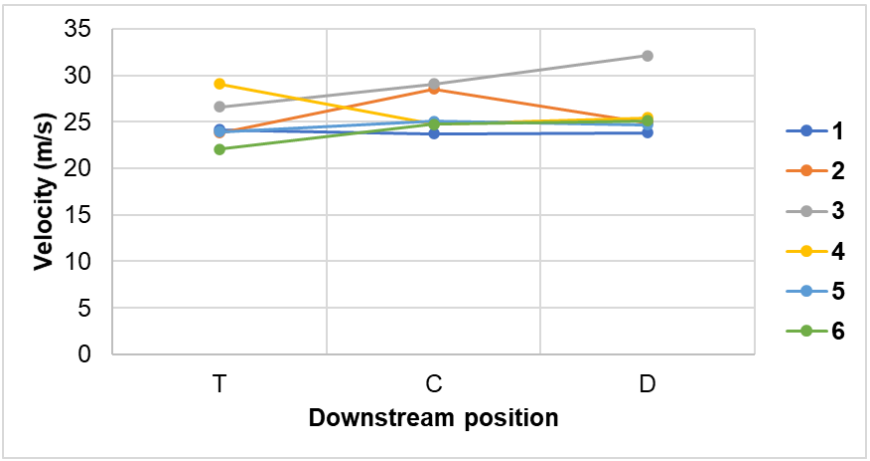

(c)

Figure 27. The measured air velocity at the three streamwise locations (T – tank, C – coupler, D – distributor) in each of the six primary hoses, at the three fan speeds: 2,200 RPM (a), 2,800 RPM (b), and 3,400 RPM (c).

For fully developed flow in a straight pipe the maximum velocity should remain consistent and at the center of the hose. The measurement location at the tank was about 0.6 m downstream of the angled portion of the steel primary tube, whereas the flexible hoses upstream of the coupler

location were relatively straight; as such, the coupler measurements were thought to be the closest condition to fully developed flow.

Aside from the distributor location for primary hoses 3 and 4, the pitot tubes were reliably placed at the center of the hose cross-section; however, this source of uncertainty is important to understand. The velocity profile through the radius of a pipe is well approximated by a power law, with n = 7, for fully developed turbulent flows (**Eq [2]**):

$$\overline{V} = \overline{V}_{max}\left(1 - \frac{r}{R}\right)^{1/n}. \qquad \textbf{[2]}$$

Taking a derivative with respect to the radial position, r, gives (**Eq [3]**):

$$\frac{d\overline{V}}{dr} = -\overline{V}_{max}\frac{1}{R\,n}\left(1 - \frac{r}{R}\right)^{\left(\frac{1-n}{n}\right)}. \qquad \textbf{[3]}$$

The sensitivity across the radius of the pipe for average coupler velocities at the three fan speeds for a pipe diameter of 63.5 mm are plotted for turbulent flow (n = 7) in **Figure 28**.

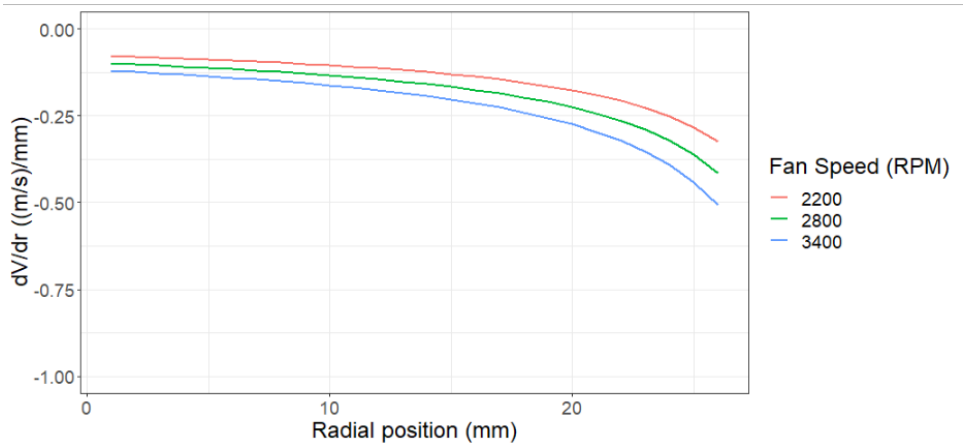

Figure 28. Sensitivity of velocity as a function of radial position, evaluated at the average measured velocity of the three fans speeds.

As an example, at the lowest fan speed, a 1 cm uncertainty in pitot tube radial position from the center of the hose would result in an error in estimation of the maximum velocity of 0.89 m/s. At the highest fan speed, the error increases to 1.39 m/s. Considering the error resulting from potential uncertainty in pitot tube positioning, the variation in the velocity between downstream positions (T, C, and D) evident in **Figure 27** is not entirely due to pitot tube placement and is suspected to be, at least in part, due to variations in hose geometry. Therefore, fully developed flow with the maximum velocity occurring at the centerline of the pipe is an overly ideal simplification of the flow behaviour in the primary hoses throughout much of the pneumatic conveying system.

The variation in flow patterns in the secondary hoses was evident in the secondary hose velocity measurements. These measurements are shown in **Figure 29** as a function of secondary hose position for distributors 4 and 6.

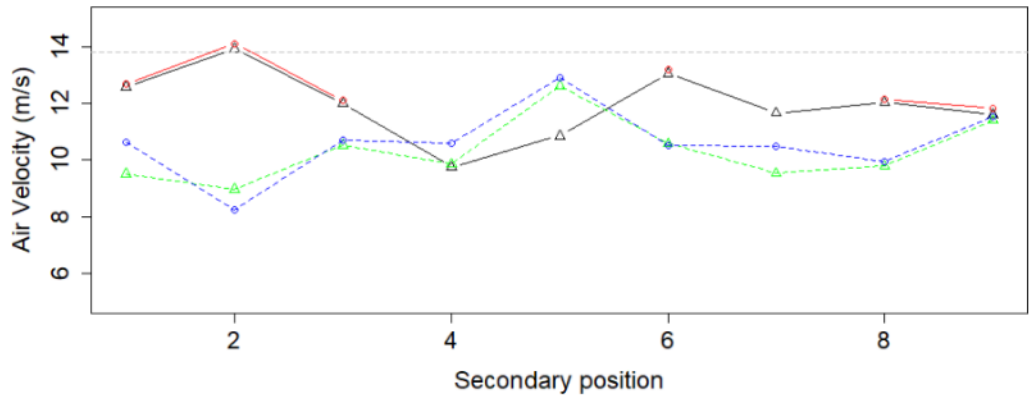

(a)

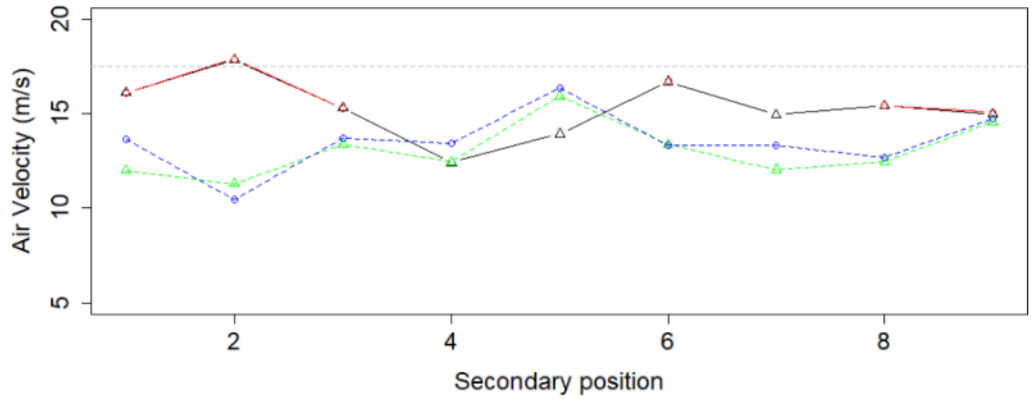

(b)

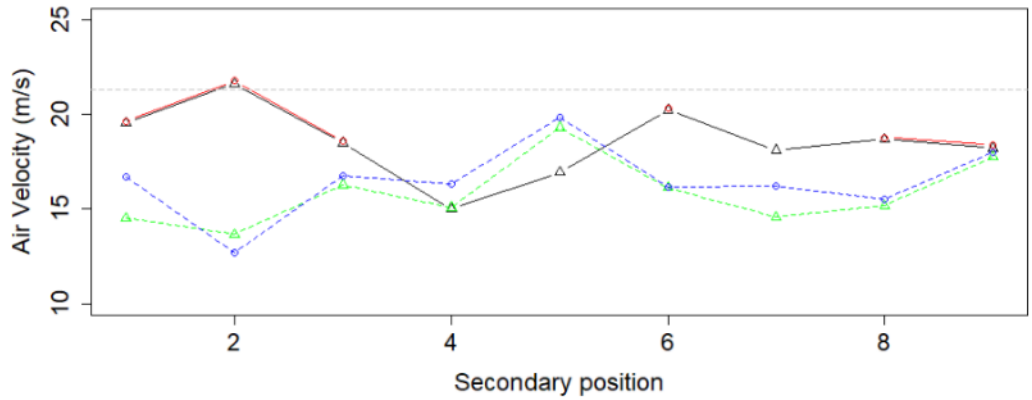

(c)

Figure 29. Velocity measurements in the secondary hoses at the three fan speeds: 2,200 RPM (a), 2,800 RPM (b), and 3,400 RPM (c). Solid red and black lines are measurements from distributor 4; dashed green and blue lines are measurements from distributor 6, with the circle and triangle symbols distinguishing between two replications. The gray horizontal dashed line represents the theoretical average velocity, based on the average measured primary hose velocities for distributors 4 and 6.

The relatively close grouping between replications for both distributors in **Figure 29** indicated good repeatability within the hoses. Furthermore, the relatively similar line shape for each distributor between fan speeds, and their respective positions relative to the theoretical average (gray horizontal dashed line) further indicated that the distribution of air between secondary hoses was relatively linear with changes in fan speed. This attribute is important, as it indicated that there likely was not a major change in the airflow patterns in the distributor.

However, the deviation of data points from the theoretical average value is difficult to interpret considering the documented difficulty with consistently installing the pitot tube at the center of the secondary hose, and the curvature of the secondary hoses upstream of the pitot tubes. Deviations from the theoretical average were likely due to both non-ideal flow distribution patterns in the secondary hose and off-centre placement of the pitot tubes.

Finally, the impact of seed being metered into the primary hoses was investigated. In **Figure 30**Figure 31, the static pressure at the tank measurement location is plotted with and without seed for primary hoses 4 and 6.

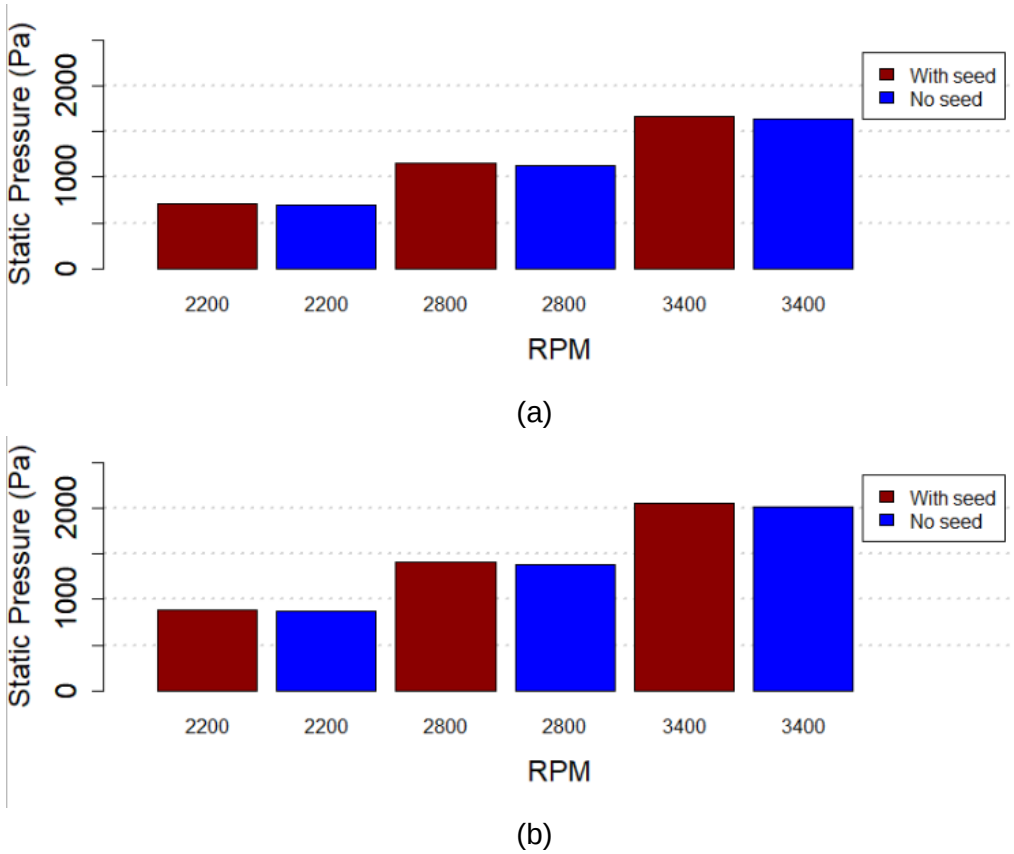

Figure 30. The static pressure with and without seed measured at the tank location for primary hose 4 (a), and 6 (b).

While detectable, the increase in static pressure due to canola being conveyed in the primary hoses was minimal. It ranged from 1.59% to 3.21% above the static pressure without canola being conveyed. At these very small solids loading ratios (SLRs; a ratio defined by the mass

flow rate of solid particles divided by the mass flow rate of the gas), ranging between approximately 0.038 and 0.059, the impact of fan speed was much larger than that of canola being conveyed.

5.4 Conclusions from Full-Scale Air Drill Testing

To investigate the relationship between seed distribution consistency and various parameters related to the pneumatic conveying system of an air drill, experiments were conducted on a John Deere 1870 double-shoot hoe drill and 1910 air cart. Air velocity and static pressure were measured in the primary hoses, and a subset of the secondary hoses. Hose lengths and routing geometry were measured as part of characterizing the equipment. Hose lengths were used in the subsequent data analysis, and the hose geometry supported the development of numerical models. Air flow measurements were taken with and without seed being conveyed. Three different fan speed treatments were used, and three replications of each treatment were completed.

Seed germination was also measured after the experiments were completed to characterize possible germination effects from pneumatic conveying; samples were grouped by distributor and fan speed treatment. No significant differences were found between the control sample taken prior to testing, and the collected canola samples. It was concluded that the germination of this canola variety (InVigor® L233P), under the given test conditions, was not affected by pneumatic conveying experiments.

Within-opener variation between runs, CV1, ranged from 0.52% to 0.71% with no strong dependency on fan speed. However, CV2 did increase with fan speed, ranging from 10.74% at 2,200 RPM to 12.57% at 3,400 RPM. The lowest fan speed (2,200 RPM) was the fan speed suggested by the operator's manual for the seed type and mass flow rate under consideration. Thus, for this air cart/drill combination under the given operating conditions, it was concluded that increasing the fan speed beyond what was suggested by the operator's manual would needlessly decrease distribution uniformity while likely increasing hydraulic power consumption. The average CV3 ranged between a minimum of 7.7% for distributor 2 and maximum of 12.1% for distributor 4; distributor 3 was excluded from comment due to the outsized CV3 value that resulted from debris becoming lodged in the distributor during testing. Further analysis indicated that within-distributor variance significantly increased with increased fan speed. This further strengthens the conclusion that, for the conditions test, operating with a fan speed greater than that suggested by the operator's manual was detrimental to the consistency of seed distribution across the air drill.

A linear model including the factors fan speed, distributor number, and secondary position, secondary hose length, and their interaction, was developed for the response variable of normalized seed mass per opener (not CV). A statistically significant model was fit ($R^2_{adjusted}$ = 0.821), where distributor number, and secondary position, secondary hose length, and their interaction were statistically significant, but fan speed was expectedly not significant. Several

conclusions were made from the results of this model. Longer secondary hoses received less seed, which suggests an influence of secondary hose length on the dividing characteristics of a distributor. Seed distribution was influenced by the angular position of the secondary hoses, which suggests a structural inconsistency in the division of seed among the distributor outlets. Additionally, the significant interaction term between secondary hose length and position factors implies that some secondary positions were more sensitive to hose lengths.

Static pressure results were largely in line with expectations; however, stronger symmetry was expected. Primary hose length effects were evident from the notably lower static pressure values for primary hoses 3 and 4. As all primary hoses are “coupled” via the common plenum at the fan, hoses that present a lower resistance should see increased airflow through them, all other factors held equal.

The measured air speed results in the primary hoses provided as much characterization of the differences in air velocity in the primary hoses as they did a commentary on the variation of airspeed across the diameter of the primary and the sensitivity of pitot tube placement. However, the differences noted in the velocity in the primary hoses was greater than the uncertainty contribution expected from potential pitot tube placement error. Based on this, it is suggested that the assumption of fully developed flow, with the maximum velocity occurring at the centerline of the pipe, is an overlay ideal simplification of the flow behaviour throughout much of a typical pneumatic conveying system.

Air velocity was also difficult to reliably measure in the secondary hoses. Future tests would benefit from installing pitot tubes in artificially straightened sections of secondary hoses at their exit from the distributor, or from an alternative measurement method (e.g., ball flow meters installed at all secondary hose outlets). Not withstanding the measurement challenges, reasonable velocity values were measured in the secondary hoses, and run-to-run repeatability was good, suggesting consistent air flow in the secondary hoses.

Finally, a small but detectable increase in static pressure due to canola being conveyed in the primary hoses occurred (1.59% to 3.21% increase above the air-only values). At these small SLRs, the impact of fan speed was much larger than that of canola being conveyed.

6. SINGLE-HOSE LABORATORY TESTING

As part of her research activities, physical testing was conducted through November 2022 in the Air-Handling Laboratory at the University of Saskatchewan by Sarita Victoria Casas Urrunaga, the M.Sc. student recruited as part of this project. The purpose of this experimental work was to investigate the impact of air speed and secondary hose length on the distribution consistency of a system with a single distributor.

The lab consisted of a centrifugal fan and control system, a seed metering system, a single primary hose up to 14 m in length, and a distributor with eight outlets. The distributor was a factory assembly produced by CNH Industrial.

A more complete description of the lab apparatus, test procedure, and results can be found in a preliminary report prepared by the student in November of 2022 provided as an addendum to this report. Final analysis and interpretation of the testing will be included as part of the student's M.Sc. thesis, expected to be finalized in 2023.

The authors of this report have provided a high-level summary of the preliminary report written by Sarita Victoria Casas Urrunaga in this section.

6.1 Experimental Methods and Materials

One seed mass flow rate (0.0031 kg/s) and multiple air speeds (13, 15, 18, 20 m/s) were tested in conjunction with three configurations of secondary hose. Trials were conducted with

1. equal-length secondary hoses (2.03 m),
2. secondary hose 5, opposite to the inlet of the primary hose to the distributor, with a length increased to 4.52 m (the longest hose on the JD 1870 air drill), and
3. secondary hoses 5 to 7 with their length increased to 4.52 m.

The distributor and secondary hoses of the lab apparatus are shown in **Figure 31**.

Figure 31. The distributor and secondary hose setup used in the lab-scale testing at the University of Saskatchewan Air-Handling Laboratory. Equal-length secondary hoses are shown in this image. Credit: Sarita Victoria Casas Urrunaga.

Additional tests were conducted with secondary hose 5, and hoses 5 and 6 blocked at their inlet in the distributor. Secondary hose lengths were held constant at 2.03 m, but the air speed was varied.

6.2 Overview of Results

CV (defined in the usual way), ranged between 9.32% and 10.36%, and increased with air speed in a statistically significant fashion. This was in close agreement to the CV2 results from the full-scales tests (**Figure 20**).

The distribution of seed for the four different configurations of hose lengths are shown in **Figure 32**. The original test numbering scheme is shown and explained in the figure caption.

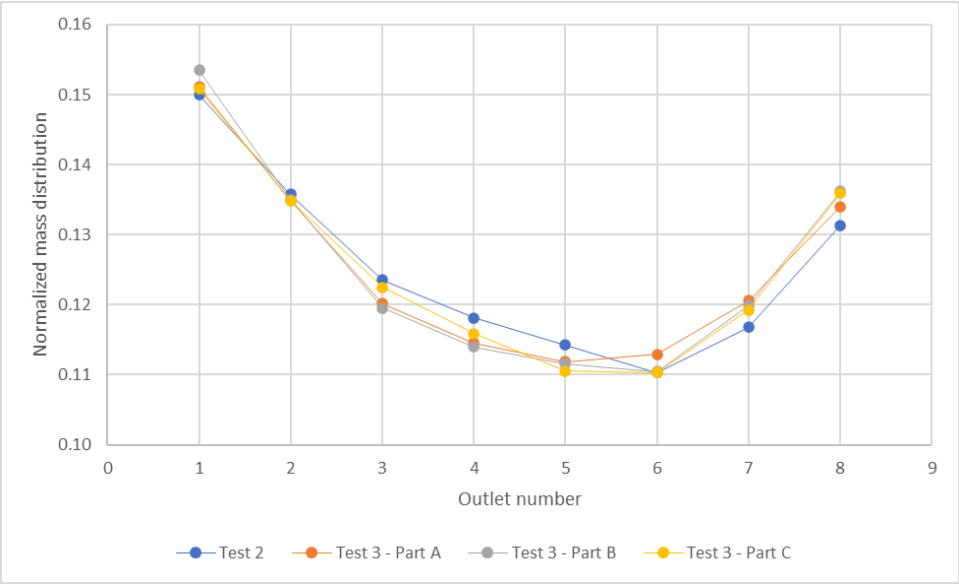

Figure 32. The normalized mass distribution of seed for the four test configurations averaged across air speed. Test 2 = equal length secondary hoses, Test 3 – Part A = hose 5 increased length, Test 3 – Part B = hose 5 and 6 increased length, Test 3 – Part C = hose 5 to 7 increased length. Source: Sarita Victoria Casas Urrunaga.

Both the imbalance based on secondary outlet position and the impact of hose length can be seen in **Figure 32**. Despite a distributor sourced from a different equipment manufacturer, controlled laboratory conditions, and controlled secondary hose lengths, and similar to the full-scale tests a consistent bias toward the secondary hose in line with the approaching primary hose and the neighboring outlets was evident. To a small degree, increasing the length of the secondary hose tended to reduce the proportion of seed that was delivered through that hose, although the impact became less clear as more hoses were lengthened.

The blockage of secondary hose 5, and hoses 5 and 6, are show in **Figure 33**.

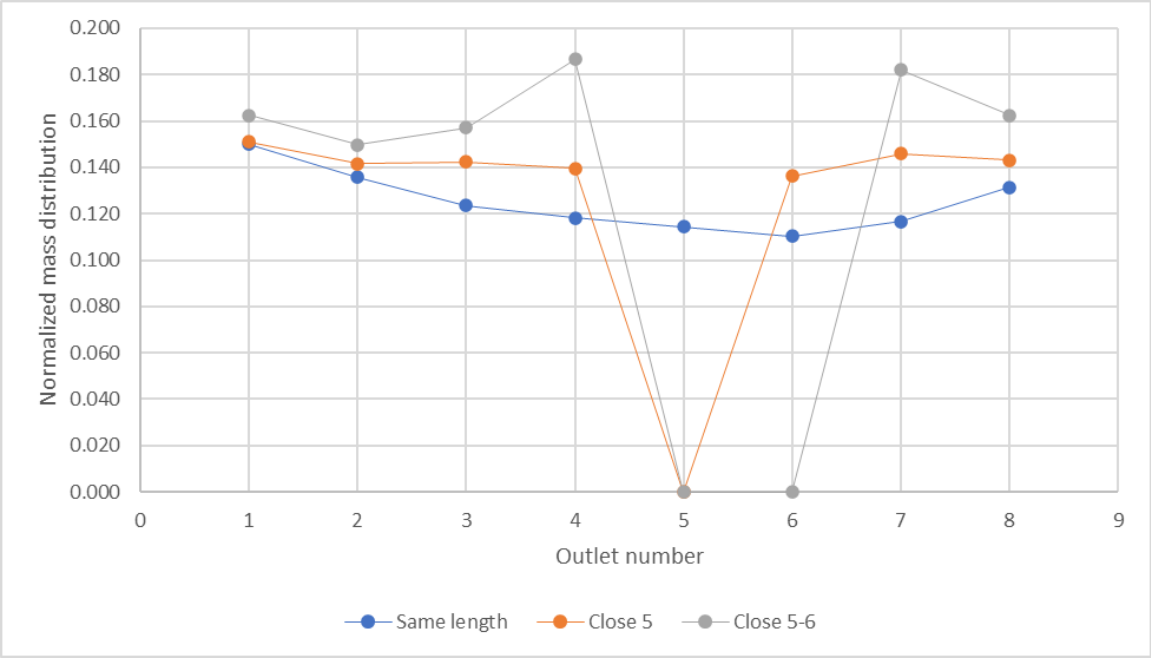

Figure 33. The normalized mass distribution of seed with no secondary hose inlets blocked ("same length"), with secondary hose 5 blocked ("close 5"), and with secondary hoses 5 and 6 blocked ("close 5-6"). Source: Sarita Victoria Casas Urrunaga.

The redistribution of seed to distributor outlets neighbouring blocked outlets is evident in **Figure 33**. A single blocked outlet resulted in the most consistent distribution among open secondary hoses, but an additional closed outlet increased the inconsistency due to a great proportion of seeds being redistributed to neighbouring outlets. As identified in the summary report, the phenomenon has been reported in the literature as being due to both changes in the pressure distribution within the distributor that promote flow, and the bouncing of seeds off the blockage surface and subsequent redistribution to neighbouring open secondary outlets (Yatskul, Lemiere, & Cointault, 2017).

6.3 Conclusions from Single-hose Testing

Laboratory testing was conducted using a single-hose pneumatic conveying apparatus that terminated in a J-tube and distributor manufactured by CNH Industrial with eight secondary hose outlets. The impact of secondary hose length on various quantities including seed mass distribution was investigated with four different configurations of secondary hose length. E length secondary hoses were tested, as well as configurations with increased hose lengths secondary 5, secondaries 5 and 6, and finally secondaries 5 - 7. The impact of closed outlets was also investigated, first by blocking the entry to secondary hose 5, then secondary hoses 5 and 6. The average air velocity in the primary hose was varied between 13 and 20 m/s, with a fixed seed mass flow rate of 0.0031 kg/s.

CV ranged between 9.32% and 10.36% and increased with air speed. These CV values were similar to the values measured during full-scale air drill testing. Overall, the greatest seed mass

fraction flowed through secondary hose 1, while position 6 typically had the lowest mass fraction (despite position 5 being diametrically opposite position 1 as this distributor had eight outlets). This slight shift could be due to swirl occurring within the vertical portion of the J-tube and into the distributor. To a small degree, increasing the length of the secondary hose tended to reduce the proportion of seed that was delivered through that hose, although the impact became less clear as more hoses were lengthened.

Blocking secondary outlets tended to redistribute the flow of seed to outlets immediately beside the blockage. When only one outlet was blocked, the overall distribution of seed mass was quite even; however, additional closed outlets resulted in the flow of seed through the neighboring open outlets to become quite high.

Overall, these experiments provided a data collection environment that permitted specific and controlled changes to hose geometries and operating conditions to support further study and model validation efforts. The presence of several trends that were also evident when testing a full-scale drill made by a different manufacturer was encouraging, as the understanding and overall conclusions of the project can be assumed to extend beyond a specific make and model of air drill.

7. SIMULATION OF PNEUMATIC CONVEYING SYSTEMS

Prior simulation and experimental work in the literature, along with the single-hose lab testing and full-scale machine testing, was used as a foundation to develop several scenarios of first an "air-only" numerical model (no seed introduced), followed by models of canola being pneumatically conveyed. The development of these models along with their comparisons to measured data and further predictions are discussed.

7.1 Air-Only Model Development

Experimental work to measure pressure gradients from Mittal (2016), along with the combination of experiments and simulations from Ebrahimi (2014) that described the velocity profile of air in round ducts, provided a foundation for the development of the air-only CFD model for the primary hoses of the pneumatic conveying system. Reynolds number (Re_D) is a dimensionless fluid velocity used throughout fluid mechanics to characterize a flow (**Eq [4]**):

$$Re_D = \frac{\rho \overline{V} D}{\mu} \quad \textbf{[4]}$$

where ρ is the density of the fluid (air), $\overline{V}$ is the average velocity of the fluid in the pipe, D is the diameter of the pipe and μ is the viscosity of the fluid.

Additionally, the power law of the velocity profile in a round duct provided an empirical description of velocity as a function or radial position. Specifically, **Eq [5]**:

$$\frac{V}{V_{max}} = \left(1 - \frac{r}{R}\right)^{1/n} \quad \textbf{[5]}$$

where V is the velocity at radial position r, V_{max} is the maximum velocity at the centerline of the pipe, R is the radius of the pipe, and n is an empirical constant taken as 7.0 for turbulent flows.

The average and maximum velocity in the pipe were related through **Eq [6]** and **Eq [7]** (White, 2006):

$$f = 0.316\, {Re_D}^{-0.25} \quad \textbf{[6]}$$

and

$$\frac{\bar{V}}{V_{max}} = (1 + 1.3\sqrt{f})^{-1} \quad \textbf{[7]}$$

where f is the Darcy friction factor, where a smooth wall was assumed throughout this work.

Also worth noting is the relationship between the volumetric flow rate, Q, and pressure drop per unit length $\frac{\Delta p}{L}$, given in **Eq [8]** (White, 2006):

$$Q = \frac{1}{4}\pi D^2 \bar{V}$$

$$\frac{\Delta p}{L} \approx\ 0.241 \rho^{3/4} \mu^{1/4} D^{-4.75} Q^{1.75} \quad \textbf{[8]}$$

The exponent of D indicates that the pressure drop predicated along a pipe is highly sensitive to its diameter, with inconsistencies and uncertainties in the pipe diameter being a potential notable source of error between measured and predicted values.

Managing the computational cost of the simulations was a consistent challenge throughout the modeling process, due to several implications:

1. Lower-cost models enable more geometry/operational configurations to be investigated for a given software license/computer asset over a fixed period of time.
2. The viability of two-way coupled CFD-DEM simulations, which would be required for heavier seeds and greater solids mass flow rates, is strongly affected by the computational cost of the CFD model, as the flow field of the fluid is recomputed at each timestep (typically hundreds of times per second of simulated time).

In CFD simulations, the fluid domain is discretized into finite volumes over which the relevant equations of momentum and mass conservation are solved numerically. These discretized volumes are referred to as the *grid*; typically, a finer grid (smaller finite volumes) permits a more accurate solution. However, more grid cells increase the computational costs to solve a given simulation (i.e., runtime, computational core count).

To capture the gradient present in the boundary layer flow against walls, the grid cells against boundaries are required to be smaller than cells located further from the wall in the rest of the flow field. However, these small cells (termed inflation layers) increase the computational cost. Using the geometry from Ebrahimi (2014), a model of a straight tube was developed to compare the impact of not using inflation layers in the grid. Meshing parameters are given in **Table 8**. The streamwise velocity profiles across the radius of the pipe (inner diameter [ID] = 0.075 m) are shown in **Figure 34**. A commercially developed CFD code, HyperWorks CFD (Altair Engineering Inc., 2021) was used throughout the project for the development and solving of the CFD results.

Table 8. Mesh parameters used to compare the impact of not using inflation layers.

Parameter	With Inflation Layers	Without Inflation Layers
Surface cell size (m)	0.005	0.005
Volume mesh size (m)	0.0075	0.0075
Minimum cell size (m)	0.001	0.004
First inflation layer cell height (m)	0.0015	-
Number of inflation layers	3	-
Total number of cells	1.37x10^6	1.12x10^6

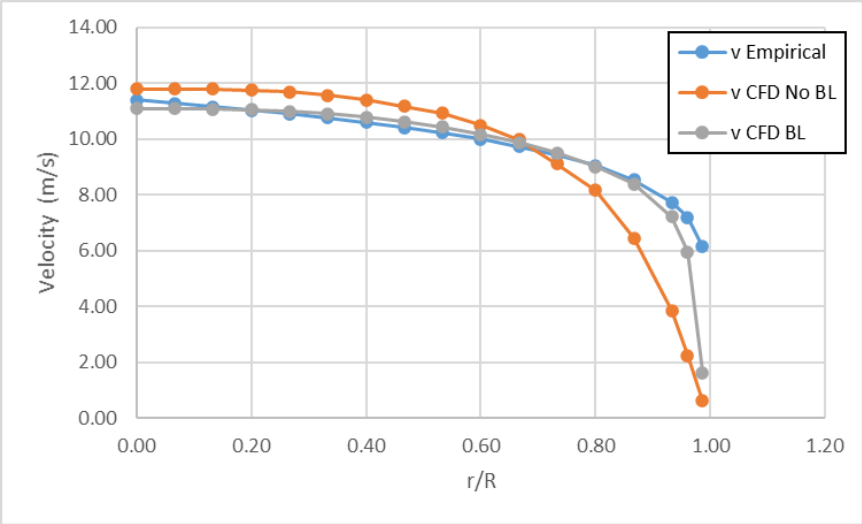

Figure 34. The streamwise velocity profile of a CFD simulation with and without inflation layer grid cells, compared to the empirical fit.

The overall agreement with the empirical solution was significantly improved with the presence of inflation layers in the grid. With inflation layers, the velocity both at the centerline of the tube (0 r/R), and near the wall (~1.0 r/R) was more accurate. The trend in the gas velocity profiles reported by Ebrahimi (2014; not shown) indicated a slight underprediction of the velocity by the empirical power law throughout much of the profile.

The simulation was also compared to experimental pressure gradient values for air-only pneumatic systems reported in the literature (Mittal, 2016). A simplified version of the experimental apparatus used in that experimental work was developed. In the experiments, wheat was pneumatically conveyed through a 57-mm ID horizontal pipe at three grain feed rates (20, 60, and 100 g/s) using air velocities ranging from 7 to 21 m/s.

Mittal (2016) concluded that the bend-angle of the test apparatus had a negligible effect on the pressure drop when only conveying air (no particles present). As an initial check of this new model geometry, an air-only condition with a 90° bend was simulated at 15 m/s. The pressure drop in the straight section of the model was approximately 45.7 Pa/m. The estimated average pressure drop through the five bend angles tested (0.0°, 22.5°, 45.0°, 67.5°, and 90.0°) ranged between from 35 to 40 Pa/m at this airspeed. The model geometry is shown in **Figure 35**.

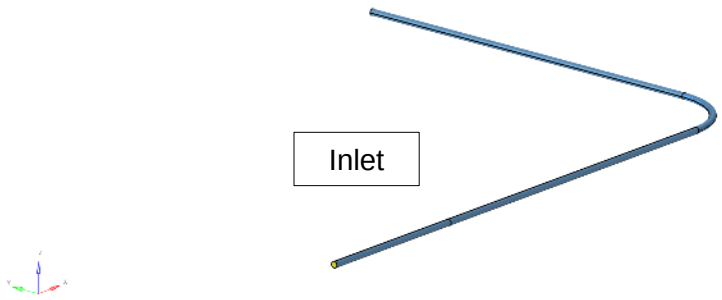

Figure 35. The geometry replicating the experimental apparatus of Mittal (2016) in the 90° bend configuration. The distance between the inlet and the start of the bend was 4.75 m. The ID of the tube was 57 mm.

CFD grid parameters from the CFD model are listed in **Table 9**.

Table 9. CFD grid parameters for the model based on Mittal (2016) experiments.

Parameter	Value
Surface cell size (m)	0.005
Volume mesh size (m)	0.010
Minimum cell size (m)	0.00075
First inflation layer cell height (m)	0.001
Number of inflation layers	3
Number of cells	1.88x10^6

Development of the CFD model then turned to the J-tube and distributor housing itself, along with the secondary hoses connected to the outlets of the distributor. The geometry was developed from measurements taken of the air cart and drill used during full-scale testing; a CAD model of the simplified geometry is shown in **Figure 36**. Note that because the fluid

domain is the meshed volume in CFD, the geometry in **Figure 36** is that of the air volume within the hoses and distributor and not of the physical components.

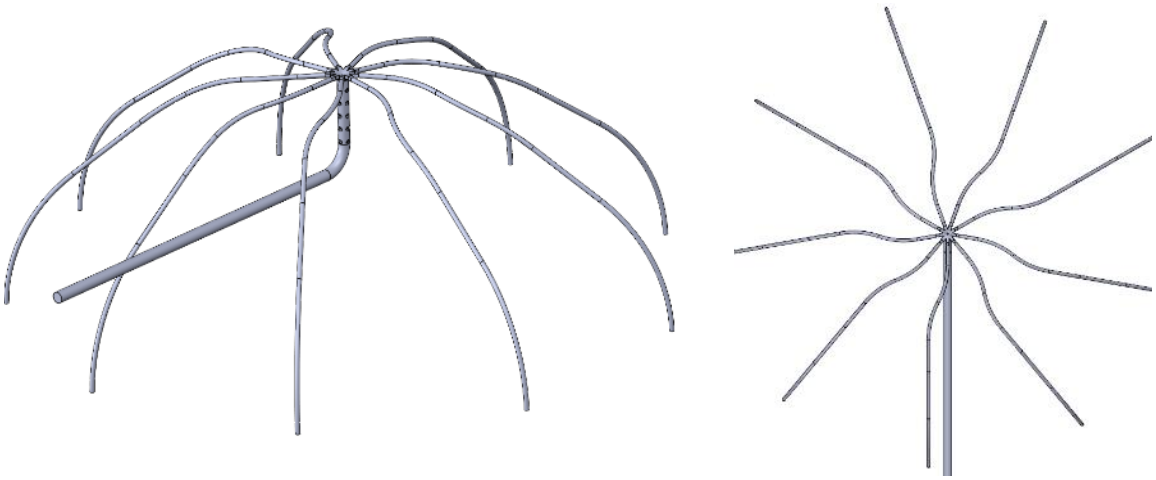

(a) (b)

Figure 36. The CAD model of a simplified primary hose, distributor, and secondary hoses for a distributor with nine outlets, viewed isometrically (a), and from above (b).

A distributor with nine outlets was simulated throughout this work as it was the more common configuration on the drill used in full-scale testing. Secondary position 1 was directly in line with the approaching primary, with numbering proceeding clockwise as viewed from above. The length of primary hose upstream of the J-tube was approximately 2.10 m. All secondary hoses were 2.40 m long.

Inlet conditions were applied to represent the measured velocity in the primary hose at the tested fan speeds, noted in **Table 10** along with additional mesh and model settings.

Table 10. Inlet average velocity boundary condition values used based on full-scale testing, and other model and mesh parameters.

Parameter	**Value**		
Fan speed (RPM)	2200	2800	3400
Inlet average velocity (m/s)	13.5	17.2	20.8
Turbulence model	RNG k-ε		
First-cell heights (mm)	Primary hose and J-tube = 1.8 Distributor = 1.0 Secondary hose = 1.5		
Max. cell size (mm)	Primary hose = 5.0 J-tube = 4.0 Distributor = 2.0 Secondary hose = 2.5		
Volume cell count	7,729,000		
Wall roughness	Smooth		

Numerical method	Reynolds-averaged Navier Stokes (RANS)

The model geometry from **Figure 36** was modified to further investigate the impact of changes in secondary hose length. Hoses for secondary positions 2 and 3 were shortened by 0.61 m (25.4% reduction from their original length), while hoses for secondary positions 8 and 9 were lengthened by 0.5 m (20.8% increase from their original length). This geometry with secondary hoses of unequal length is shown in **Figure 37**.

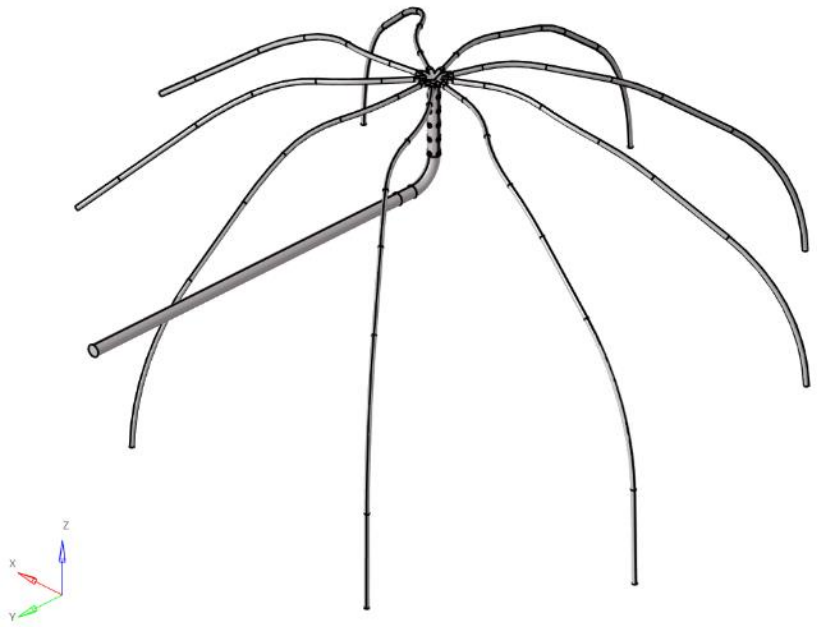

Figure 37. The distributor modified to have shorter primary hoses 2 and 3, and longer primary hoses 8 and 9.

Finally, a CAD facsimile of the pneumatic conveying system of air drill used during full-scale test was developed from dimensions gathered during the testing; the model is shown in **Figure 38**. Being that the routing of the primary hoses was reasonably symmetrical, only the routings on the right-hand side of the machine were modeled. Secondary hose lengths were modified to match those measured on the air drill used for full-scale testing, summarized in **Table 1**.

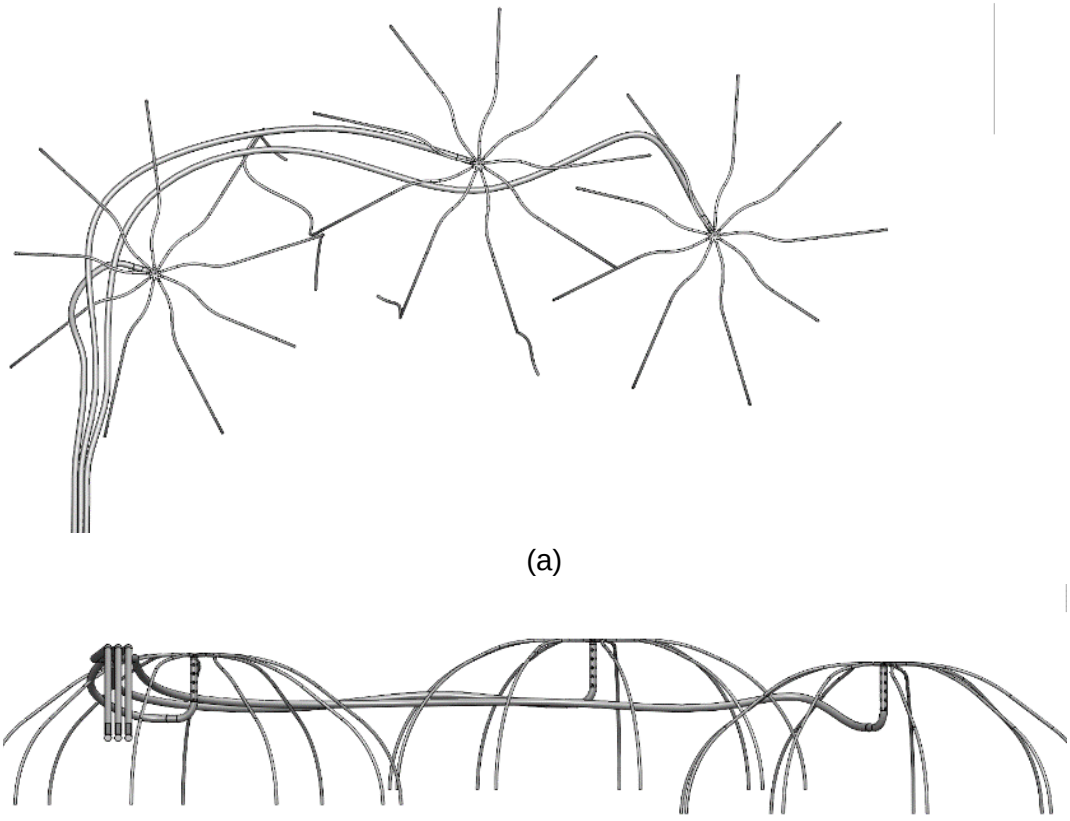

(a)

(b)

Figure 38. Hose geometries for primary hoses 4 to 6 based on the John Deere 1870 air drill used in full-scale testing, viewed from above (a), and from behind the drill looking forward (b).

The layout of the primary hoses includes several bend features of interest. Primary hose 4 (the left-most primary and distributor in **Figure 38**) includes a sudden elevation change and a sharp turn immediately upstream of the distributor tower. Primary hose 5 (the central primary hose and distributor in **Figure 38**) has gentle sweeping bends with a relatively straight approach to the distributor tower. Primary hose 6 contains sweeping bends with a pronounced 90° bend upstream of the distributor tower, albeit at a greater distance upstream of the distributor than primary hose 4.

7.2 CFD-DEM Model Development for Canola Pneumatic Conveying

While the insights gleaned from an air-only model can be illustrative of the fundamental performance of a pneumatic conveying system, simulating the transport and distribution of solid particulate ultimately requires a representation of the solid particles to be included in the simulation of the system. Multiple solid-gas simulation approaches exist; this can range from a two-fluid model, where the solids phase is abstracted as a second fluid, to the discrete representation of each particle, including its interaction with both walls and other particles present in the model, by using the discrete element method (DEM). Discrete element method

models were developed in the commercially available software EDEM (Altair Engineering Inc., 2021).

Pneumatic conveying applications in agriculture typically involve relatively large particles with non-negligible inertia that are also influenced by interactions with wall boundaries and other particles. Thus, the need to use a DEM representation of particles at least partially coupled to a CFD flow field of the gas was identified early in the project. After this, the need to simulate the flow field, model the canola using a DEM approach, and determine an appropriate means to communicate the forces between the particles and the gas became the natural tasks required to develop a pneumatic conveying model of canola. The development of the flow field simulation was discussed in **Section 6.1**. The representation of canola using DEM, and the coupling between DEM particles and the CFD flow field are discussed below.

Values for the physical characterization of canola, along with DEM particle-particle and particle-wall interaction parameters were taken from the literature (Boac, Casada, Maghirang, & Harner III, 2010). The specific values used in our simulations are given in **Table 11**. It is noted that the sensitivity of the simulation results to the particle-wall interaction parameters was not investigated during the course of this work. However, given the potential range of interaction values for both the non-metallic hoses produced by several vendors, and the influence of the wide range of potential surface conditions of the metallic and non-metallic hoses in in-service air drill systems, the interaction values used likely represent but one of the many possible appropriate values for this aspect of the simulations.

Table 11. DEM parameters used in the simulation of canola in an air seeder.

Parameter	Value
Particle density (kg/m^3)	1100
Particle Poisson's ratio	0.4
Particle shear modulus (MPa)	10.0
Particle-particle coefficient of restitution	0.6
Particle-particle coefficient of static friction	0.5
Particle-particle coefficient of rolling friction	0.005
Particle-hose coefficient of restitution	0.6
Particle-hose coefficient of static friction	0.3
Particle-hose coefficient of rolling friction	0.005

When coupling CFD and DEM simulations, a choice between *one way* and *two way* coupling between the simulation engines is required:

- One way coupling: aerodynamic forces of the fluid flow acting on a particle are communicated to the particles during the simulation. This results in the particle being influenced by the given features of the flow field. However, the impact of the particle on the flow field (e.g., momentum transfer, turbulence modulation, mass conservation implications

from particle introductions) are not included in the simulation. A static CFD solution can be solved first, and subsequently used to calculate aerodynamic forces on particles as they travel through the system.
- Two way coupling: in addition to the aerodynamic forces being transferred onto the solid particle phase, the solid particle phase is recognized within the CFD simulation and both evolution of the fluid and particle flows develop simultaneously. These simulations are inherently transient.

While two-way coupling provides a more complete representation of the two-phase system, it requires the CFD and DEM models to run and solve simultaneously. This is typically orders of magnitude greater in terms of computation cost in comparison to a one-way coupled model. Due to the low solids loading ratio and the relatively small size of canola seeds, one-way coupling was used throughout the modeling of the pneumatic conveying of canola in this work.

Ebrahimi (2014) identified the importance of including the Magnus lift force when modeling the pneumatic transport of spherical particles. This lift force model, based on the angular velocity of a particle, along with the Saffman lift model and the Schiller-Naumann drag force model, were used throughout the simulations herein in order to communicate the aerodynamic forces from the fluid flow field onto the particles.

As one-way coupling was selected to communicate the aerodynamic forces onto the canola particles, the velocity and vorticity fields computed in the air-only simulations developed in **Section 6.1** were exported and reused during the simulation of canola particles traveling through the pneumatic conveying system. EDEM (Altair Engineering Inc., 2021) was used as the DEM simulation tool; capability internal to EDEM enabled the calculation of aerodynamic forces acting on every particle introduced into the system. In the DEM these forces are then integrated through time, along with particle-particle and particle-wall collision forces, to predict the trajectory of the particles through the system of interest.

Particle creation was based on the seeding rate used during testing of the full-scale air drill, the typical “5 lb/ac at 5 mph”. The thousand kernel weight for the particular seed tested was 4.7 g. When calculated out, this resulted in a solids mass flow rate of 0.003 kg/s per primary hose leading to a distributor with nine secondary outlets.

7.3 Results and Discussion

The behaviour of both an air-only CFD model and a two-phase CFD-DEM model (albeit, with one-way coupling) was of interest, as it was anticipated that the behaviour of the fluid phase would play an important role in the distribution performance of an air drill, especially when conveying canola. As such, the results from air-only simulations are presented in **Section 6.3.1**. Results from the generic distributor in **Figure 36** are discussed first, along with the impact of secondary hoses with unequal lengths (geometry shown in **Figure 37**). The modeling method

was then applied to a facsimile of the geometry of the JD 1870 air drill where primary runs 4 and 6 were simulated. Particles were then introduced into these fluid flow results in in **Section 6.3.2** in order to develop an understanding of the impact of various flow field features on the distribution performance of the systems.

7.3.1 Air-Only Simulations

Overall, the air-only simulations were characterized by the evolution of fully developed pipe flow in the straight portion of primary hose leading up to the J-tube of the distributor, followed by the transition of flow through the bend of the J-tube, the impact of the dimples in the vertical portion of the distributor pipe, and finally the division of flow in the distributor head itself. A cross section of the velocity profile through both the vertical centerline of the primary pipe and in a horizontal plane through the distributor with equal-length secondary hoses is shown in **Figure 39**. Due to the odd number of secondary hoses and the bend in secondary 1, a limited portion of the flow field in the secondary hoses is shown. Very similar flow patterns were present for all three of the simulated fan speeds; as such, the results for a fan speed of 2,200 RPM were focused on throughout the report for brevity.

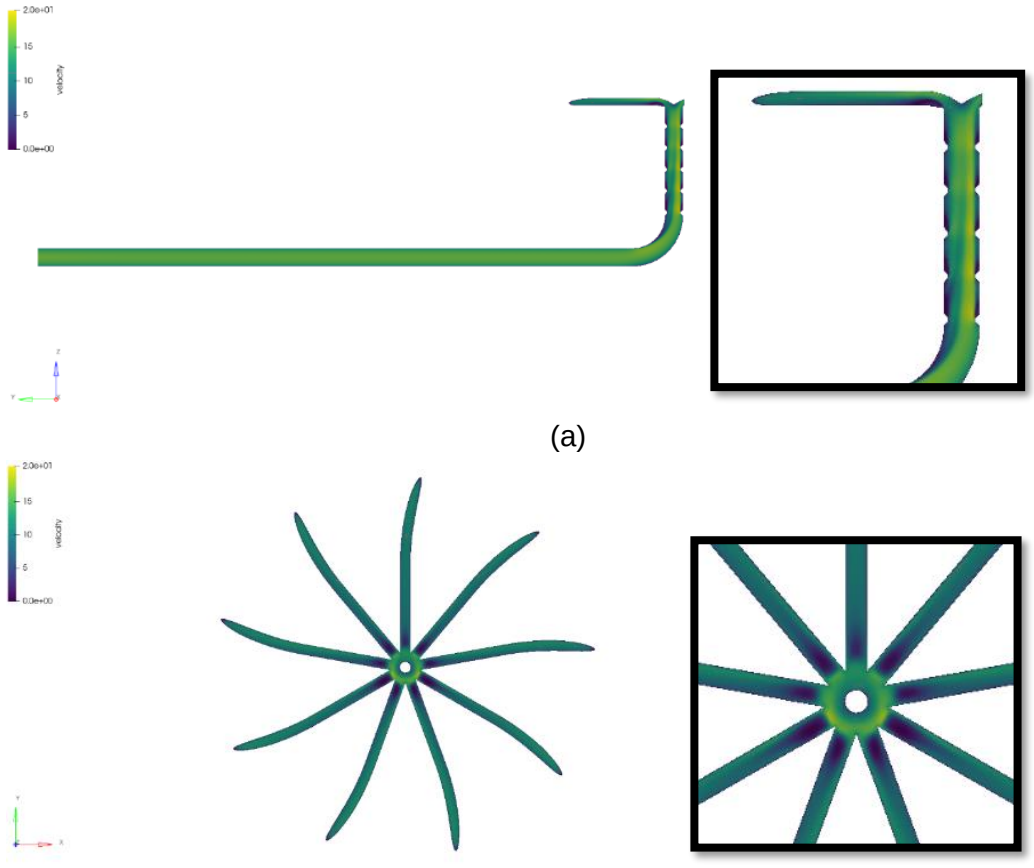

Figure 39. The velocity profile through the vertical center plane (a), and a horizontal plane through the mid-height of the secondary hose outlets of the distributor (b), with zoomed-in views to the right of each set. The boundary conditions were based on 2,200 RPM. In (b), the primary hose approaches from the +y direction (top of the image) making secondary hose #1 point toward the 12 o'clock position.

Several important flow features can be seen in **Figure 39 (a)**. In the bend of the J-tube, flow separation from the inside (+y) of the elbow can be seen as a slow stagnant region forms between the inside of the curve and the first dimple. Dimples on the -y side of the vertical tube shift the greatest velocity toward the center of the tube, although the bias of the profile emanating from the outside of the bend remained evident. Separation due to the dimples all the way up the tube was evident from the regions of low velocity immediately downstream of them.

Flow separation in the entry into the secondary hose can be seen in **Figure 39 (a)** due to the sharp transition. This is further evident in the inconsistent air velocity pattern along the length of each secondary hose near the distributor in **Figure 39 (b)**. A higher velocity was present near the outlets on the -y half of the distributor, with the greatest velocity in the cross section present at secondary hoses 4 and 7. To investigate this further, an additional cross-sectioning plane was added to visualize the flow pattern through the central vertical plane of secondary hose 5. This is shown in **Figure 40**.

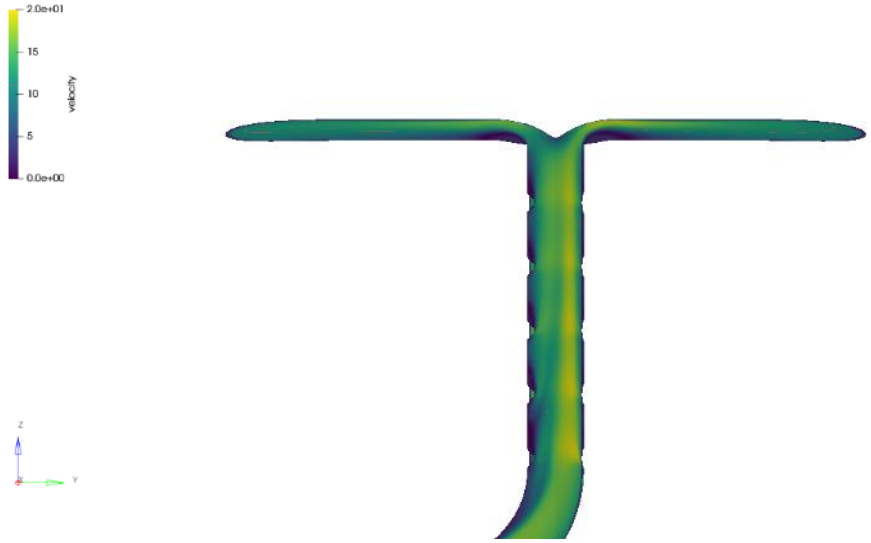

Figure 40. Velocity in both secondary hoses 1 and 5, left and right primary hoses, respectively, at 2,200 RPM with the primary hose again approaching from the left of the image.

Due to the increased velocity at the entry of the transition to secondary hose 5, a larger separation from the bottom of the secondary hose formed. Despite the larger region of flow separation, the pattern of the mass flux at the outlet of each secondary hose, shown in **Figure 41**, indicated that more air flows through secondary hoses 4 to 7, although the flow division was relatively consistent. Secondary hoses 2 and 9 had the lowest air flow rate.

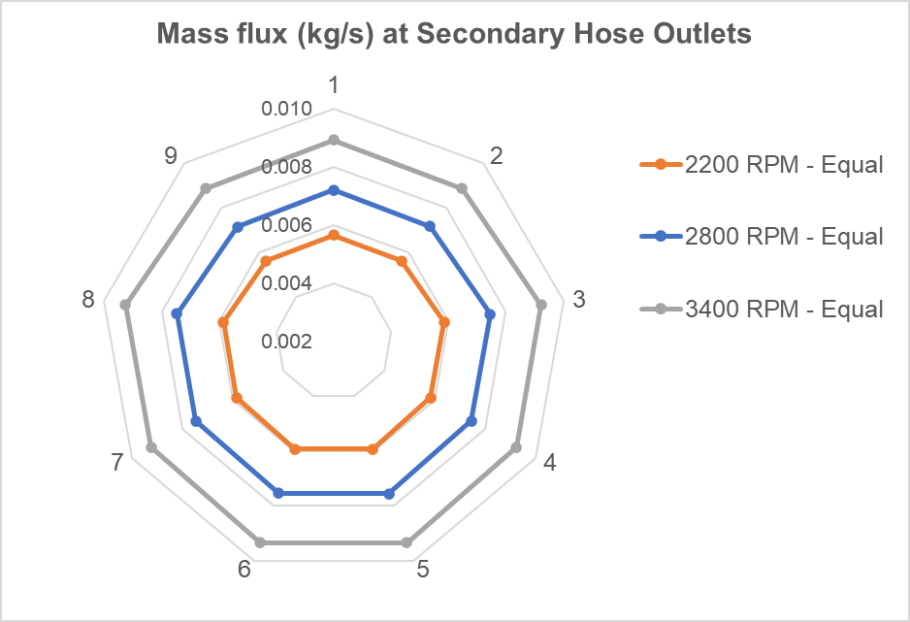

Figure 41. Mass fluxes at the secondary hose outlets for the three simulated fan speeds for the equal-length secondary hose geometry.

The differences in outlet mass flux indicated in **Figure 41** highlight that, all other factors held equal, preferential flow paths can result in modern air drills. Furthermore, it highlighted that the J-tube elbow influenced the airflow pattern within the distributor head itself.

The bias in airflow was further visualized by generating an iso-surface based on velocity results from the simulations. In **Figure 42** and **Figure 45**, an iso-surface was created for a velocity magnitude value of 15.0 m/s. The colouring of the surface was based on the pressure results coincident at the iso-surface. Note that since the velocity approached 0 m/s at the wall, the region within the iso-surface had a velocity of 15.0 m/s or greater.

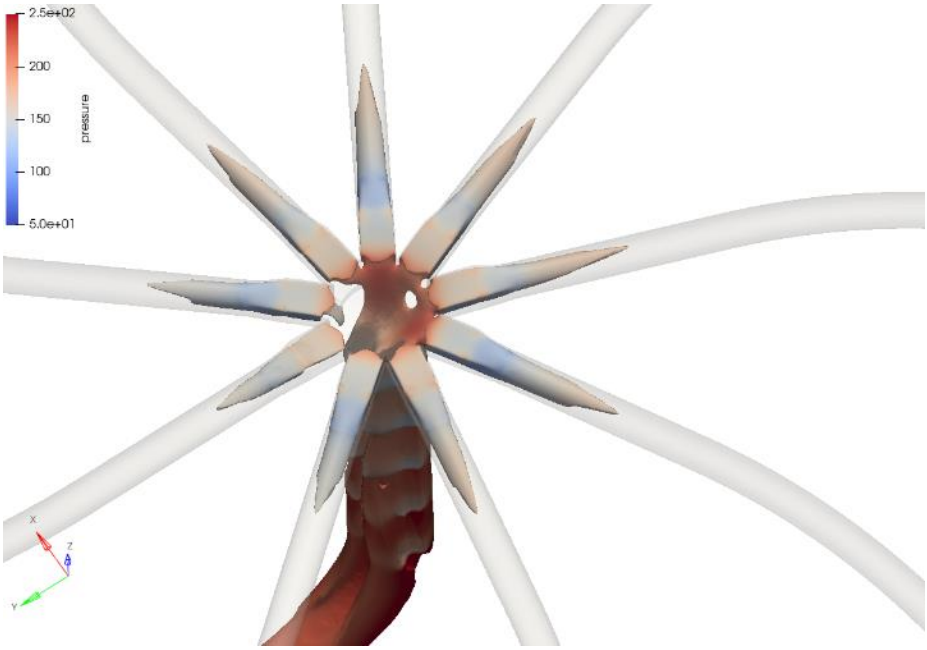

Figure 42. A velocity magnitude iso-surface rendered at 15.0 m/s, coloured by static pressure, for the equal-length secondary hoses model simulated at 2,200 RPM. Secondary 1 extends toward the bottom left corner of the image in the +y direction.

Inconsistency in the distribution of airflow was evident based on the different sizes of encapsulated volume extending into the secondary hoses. A continuous volume extended from the J-tube into secondary hoses 4 to 7, indicating the higher velocity of fluid entering those hoses as identified earlier.

Although some inconsistency in air flow can be attributed to the geometry of the system, when the results of **Figure 41** are plotted in terms of air mass fraction (i.e., outlet mass flux normalized by total outlet mass flux), the response of the simulated system was very consistent across changes in fan speed. Outlet mass fractions are plotted in **Figure 43**.

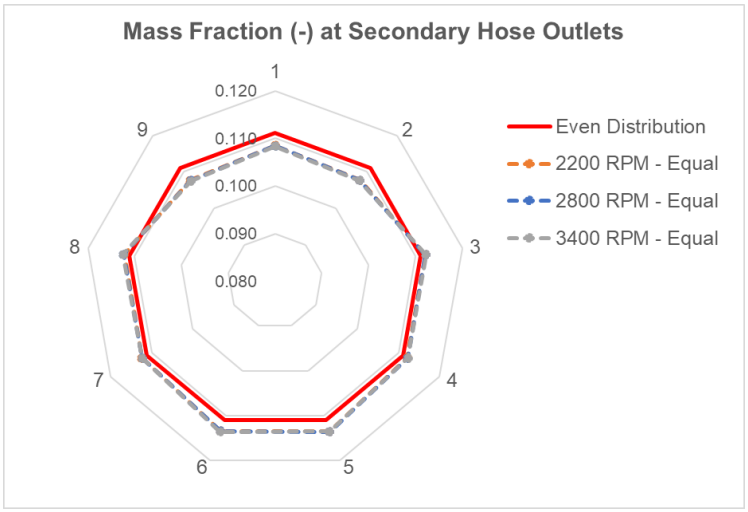

Figure 43. Air mass fraction at the secondary hose outlets for the three simulated fan speeds for the equal-length secondary hose geometry.

This linearity with inlet mass flux was encouraging, as it indicated that changes with fan speed do not lead to major changes in flow regimes within the conveying system. Linearity provides an element of predictability in the operation of the conveying system. The ratio of maximum to minimum air mass fraction was 1.06 for all three speeds; this indicated that the variation in air mass fraction between secondary outlets was quite low.

The effect of changes in secondary hose length on flow distribution were explored with the model geometry featuring unequal secondary hose lengths shown in **Figure 37**. Simulations were run in a similar fashion with the inlet conditions based on the three different fans speeds. The mass fluxes at the secondary hose outlets with this geometry are plotted overtop of the equal-length secondary hose results in **Figure 44**.

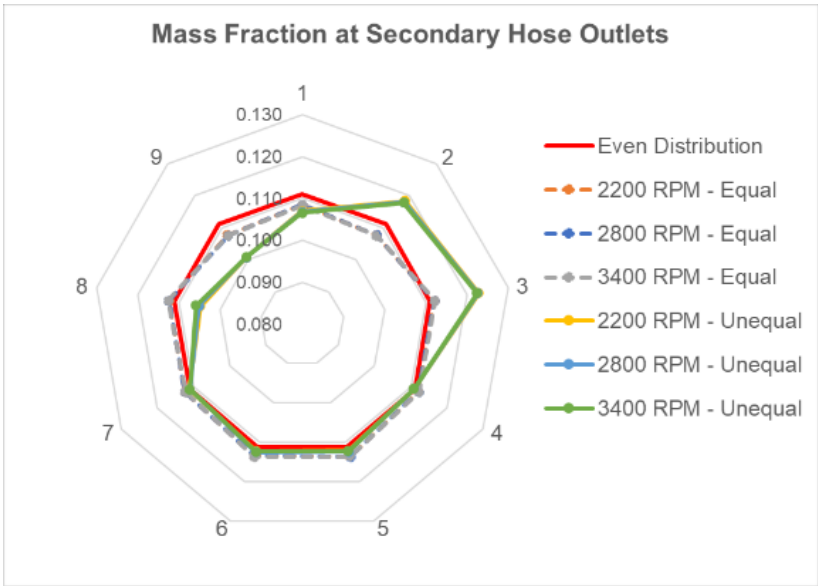

Figure 44. Air mass fraction at the secondary hose outlets for the three simulated fan speeds for the secondary hoses with differing lengths compare to the equal-length results in **Figure 41**.

Flow was biased toward the shorter hoses and away from the longer hoses at all three fan speeds. The changes in secondary hose length were effectively additive to the inconsistency already evident in **Figure 43**, in that the air mass fraction at positions 3 and 8 was greater than that at 2 and 9, respectively. With the unequal length secondary hoses, the ratio of maximum to minimum air mass fraction was 1.22 for all three speeds.

A velocity magnitude iso-surface was generated from the simulation based on 2,200 RPM, again for a velocity magnitude of 15.0 m/s, shown in **Figure 45**.

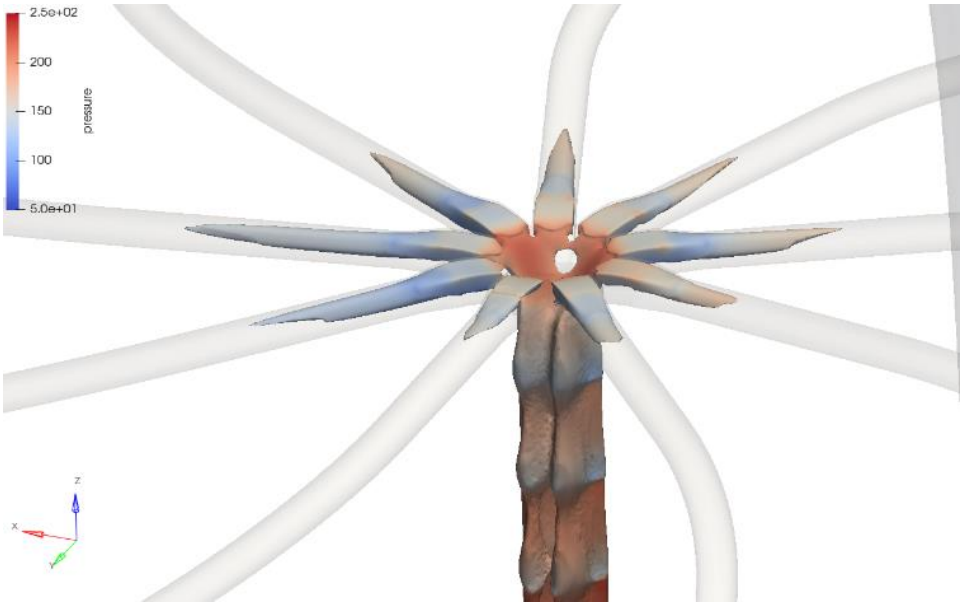

Figure 45. A velocity magnitude iso-surface rendered at 15.0 m/s, coloured by static pressure, for the unequal secondary hose length simulated at 2,200 RPM. Secondary 1 extends toward the bottom left corner of the image in the +y direction.

The iso-surface results illustrate a greater mass flow toward secondary outlets 2 and 3 in comparison to 8 and 9, as a larger volume of the flow is within the iso-surface (and therefore has a velocity of 15.0 m/s or greater).

Airflow through the model based on the air drill used for full-scale was also simulated. The impact of the curvature of the primary hoses was of interest, given the simplified geometry of the primary hose in the ideal distributor models in **Figure 36** and **Figure 37**.

Individual models for primaries 4 to 6 were simulated. Velocity streamlines for primary 4 are shown in **Figure 46**, as viewed from above and to the left of the transition from the air cart to the drill.

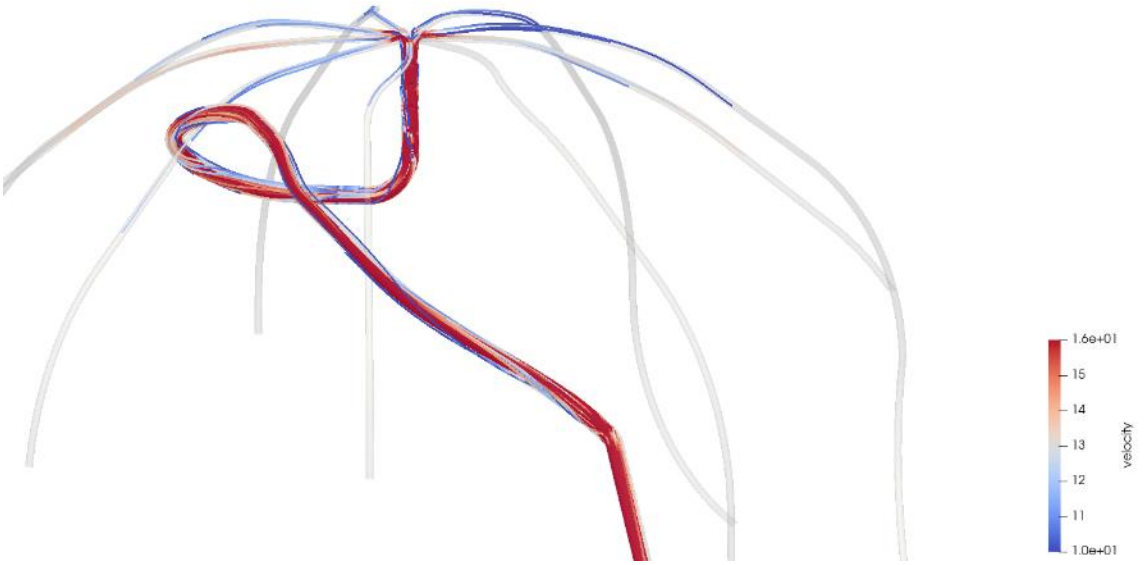

Figure 46. Velocity streamlines for primary 4 simulated at 2,200 RPM, as viewed from above and to the left of the transition from the air cart to the drill.

The impact of the various bends in primary are evident in **Figure 46**. Common to all three primary hoses simulated, the angled riser tube at the front of the air cart did create a disturbance due to flow separation along the bottom of the pipe that resulted in some rotation of the streamlines along the axis of flow. Further downstream, the tight curve and elevation change present in primary 4 modified the flow conditions upstream of the entry to the J-tube. **Figure 47** is a more detailed view of this behaviour.

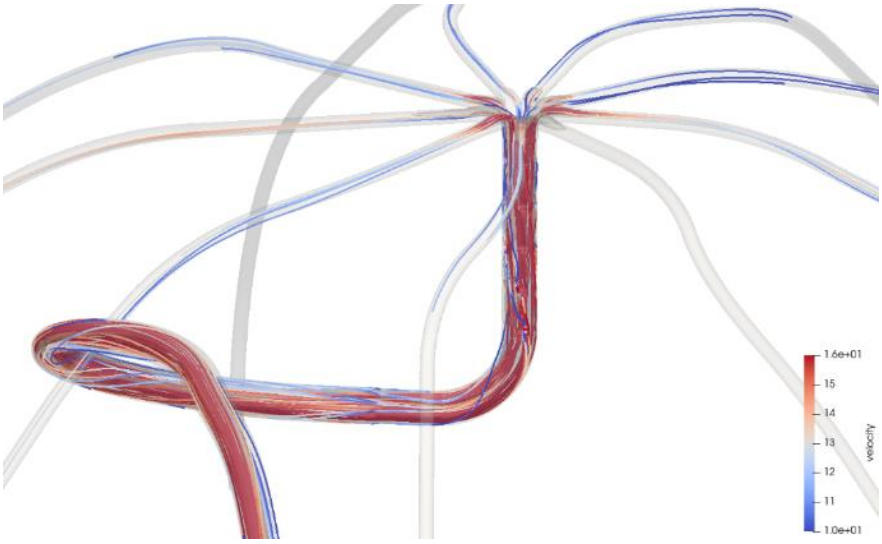

Figure 47. A detailed view of the flow behaviour through the sharp bend in primary 4 upstream of the entry to the distributor J-tube.

The velocity reduction along the inside of the primary hose bend, combined with the elevation change generated some rotation in the flow prior to entering the J-tube. However, the dimpling in the J-tube walls tended to suppress the rotation while increasing turbulence, assumed to promote mixing of the seed across the diameter of the J-tube before entering the distributor.

An iso-surface of velocity magnitude in the distributor at 14.0 m/s is shown in **Figure 48**. Here, significant imbalances in air velocity at the outlets to the secondary hoses are evident.

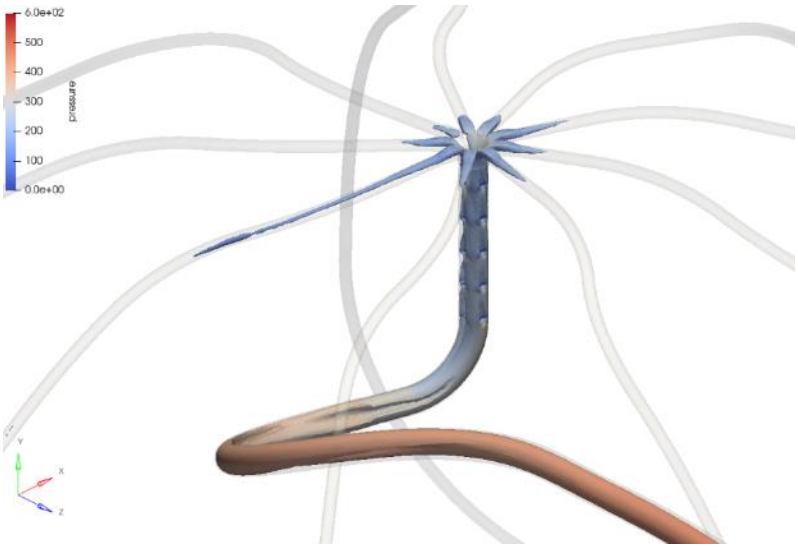

Figure 48. Velocity iso-surface at 14.0 m/s through primary 4 simulated at 2,200 RPM.

The secondary hose containing the largest encapsulated volume of flow field is secondary 1 on this distributor.

Streamlines generated upstream of distributor 6, shown in **Figure 49**, illustrated the effect of greater bend radii in primary hoses: flow separation was less severe in this primary hose.

Figure 49. Streamlines upstream of distributor 6 simulated at 2,200 RPM.

The hose geometry in **Figure 49** also highlighted the impact of the proximity of a bend to the entry to the distributor. Overall, greater bend radii further upstream of the J-tube entry aided in smoothing out the flow upon entering the J-tube and distributor.

Similar to the earlier analyses, air mass fraction at each outlet provides the clearest indication of flow through each secondary hose. This value is plotted for the three distributors modeled (4, 5, and 6) in **Figure 50**.

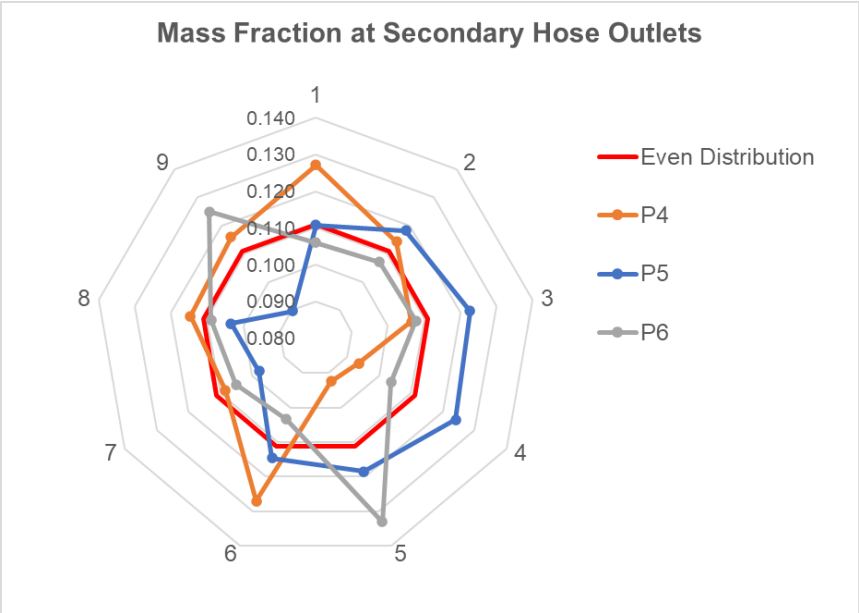

Figure 50. The air mass fraction at the secondary hose outlets (secondary hose air mass flux normalized by the total outlet mass flux) for primary hoses 4 to 6 based on a simulated fan speed of 2,200 RPM.

In comparison to the theoretically even distribution, the mass flux varied significantly with the secondary outlet position; however, when these mass fraction values were plotted against the length of each secondary hose in the model in **Figure 51**, a noticeable trend of decreasing mass fraction through longer secondary hoses was evident.

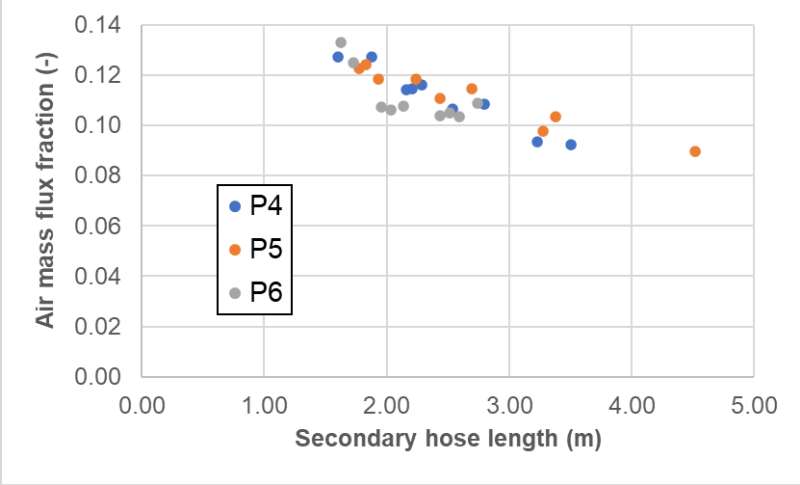

Figure 51. Air mass fraction through each secondary hose in primary 4 (P4), 5 (P5), and 6 (P6) plotted against the modelled length of each secondary hose.

The single-hose laboratory testing, and the simulations comparing equal and un-equal length secondary hoses provided a controlled illustration of the impact of secondary hose length. Based on the results in **Figure 51** and preceding visualizations, secondary hose length remained a notable factor in the consistency of airflow in the more complicated geometry that was based on the full-scale drill.

7.3.2 Canola Pneumatic Conveying Simulations

As the velocity and vorticity fields computed in the air-only simulations discussed in **Section 6.3.1** were reused during the simulation of canola particles, we present and discuss the results from the pneumatic conveying models in a similar progression below. The idealized secondary with secondary hoses with equal length is discussed first, followed by the impact of unequal length hoses. Finally, select results from simulations of the full-scale pneumatic conveying system are discussed.

In the model shown in **Figure 36** with equal length secondary hoses, particle flow developed through approximately the first half of the primary pipe and particles tended to travel in the lower half of the pipe cross section prior to entering the J-tube, as shown in **Figure 52**.

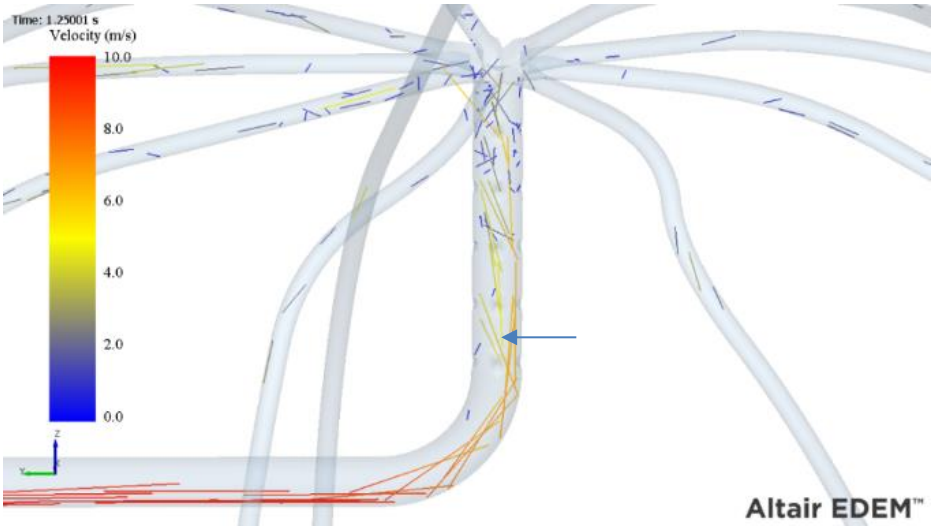

Figure 52. Canola particle travel paths colored by velocity with the airflow based on 2,200 RPM through the system with secondary hoses of equal length. The blue arrow indicated the location of the lowest dimple on the back (-y) side of the J-tube.

Some canola particles impacted the outside curve of the J-tube elbow and then bounced upward and into the front side (+y) side of the tube. Other particle tended to slide along the elbow, with many of the particles impacting the first dimple on the back (-y) side of the tube. Impact with the lowest dimple scattered particles into the center of the pipe where their velocity remained relatively high. Despite the analysis of the air-only results indicating greater portion of air flowing through the secondary hoses opposite the J-tube elbow (see **Figure 43**), the particles that maintained a relatively high velocity through the center of the vertical tube tended to pass through secondary outlets on the same side as the J-tube elbow (secondary hoses 1, 2, and 9).

Simulations were also conducted using the airflow results for the other fan speeds; each DEM simulation was run for 15.0 seconds of model time. The seed mass through each secondary outlet was measured during each simulation. The mass seed fraction through each secondary hose is plotted in **Figure 53**.

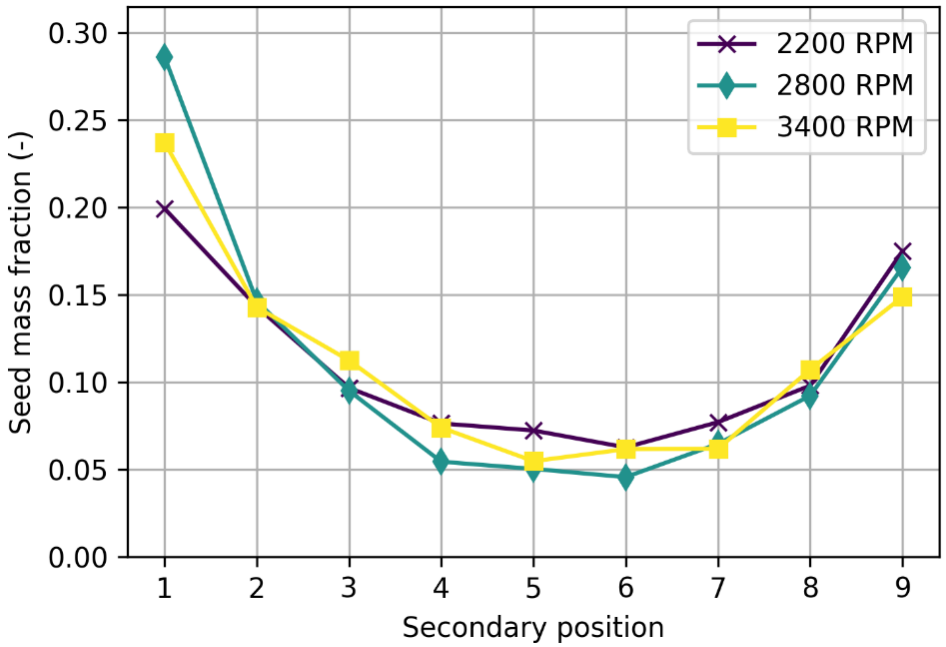

Figure 53. Seed mass fraction through each secondary hose with secondary hoses of equal length, during the three fan speeds simulated.

In comparison to the seed mass fraction result from the single-hose laboratory testing shown in **Figure 32**, the variation between minimum and maximum seed fraction was greater in the simulations. The range of experimental mass fraction ranged from 0.11 to 0.155, while the range from simulations results was between 0.05 and 0.21. However, the trend was very similar. Despite preferential air flow to secondary hoses 4 to 7, more seed mass passed through the secondary hoses on the side of the distributor aligned with the entry of the primary hose (secondary hoses 1, 2, and 9). The distribution consistency was best at the lowest fan speed, but the trend shown in the experimental testing of increasing variance with increasing fan speed was not as apparent in the simulation results.

To some surprise, the airflow imbalance toward shorter secondary hoses resulting from the model geometry shown in **Figure 37** resulted in a much more even distribution of seed division in the pneumatic conveying model of canola. The seed mass fraction from these simulations are plotted in **Figure 54**, in addition to the results from **Figure 53** for comparison.

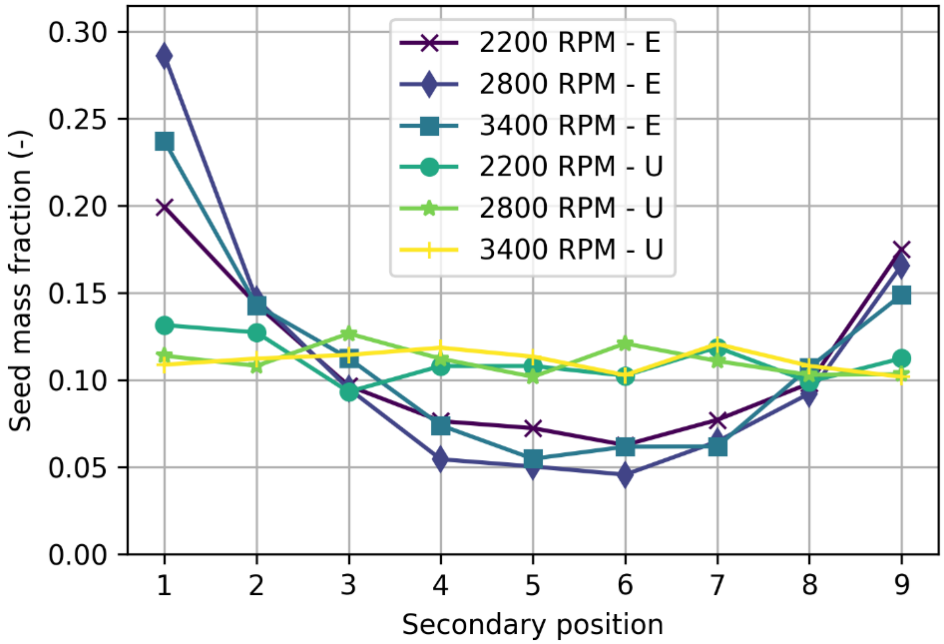

Figure 54. The seed mass distribution results with the simplified distributor geometry with unequal length secondary hoses (U) where secondary hoses 2 and 3 were shorter and hoses 8 and 9 were longer are overlaid on the results from equal length hoses (E), at three simulated fan speeds.

These results suggested that without the interaction of variations in secondary hose length and position to create asymmetries within the airflow patterns in the J-tube and distributor, the fundamental flow pattern that results from equal length hoses results in biased seed distribution characteristics. While these results are a potentially unintuitive result at first consideration, the difference between where air most easily flowed through (secondary outlets 4 to 7) compared to where seed most easily flow through (outlets 1, 2, and 9) with equal length secondary hoses was already indicative that the trajectory of particles was not guaranteed to follow preferential airflow paths through a pneumatic conveying.

Overall, the simulation results do appear more sensitive to secondary hose length changes in comparison to the single-hose laboratory testing results briefly discussed in **Section 6.2**. Further interpretation is difficult due to different secondary hoses being modified in the student's experiments compared to the simulations above; however, the simulations with geometry based on the air drill used during full-scale testing can also be studied. The mass fraction of seed as a function of secondary hose position for primary hoses 4 and 6 are shown in **Figure 55**.

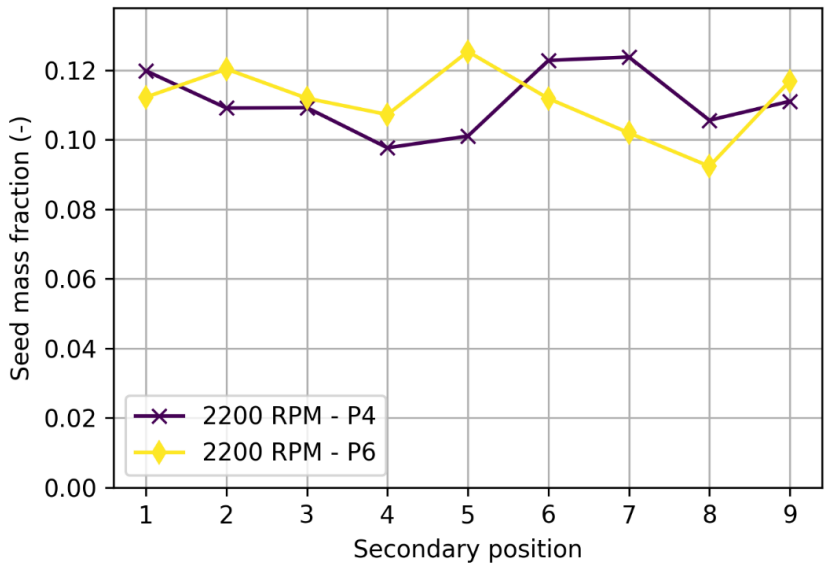

Figure 55. The simulated seed mass fraction through the secondary hoses of primary 4 (P4) and 6 (P6) of the modeled full-scale drill, at a fan speed of 2200 RPM.

Similar to the results from the ideal distributor geometry, the impact of variations in secondary hose length were evident in the simulations of the primary hose geometry based on the John Deere air drill used during full-scale testing. This was investigated through by plotting the mass fraction results of **Figure 55** against the length of the secondary hoses; these results are shown in **Figure 56**.

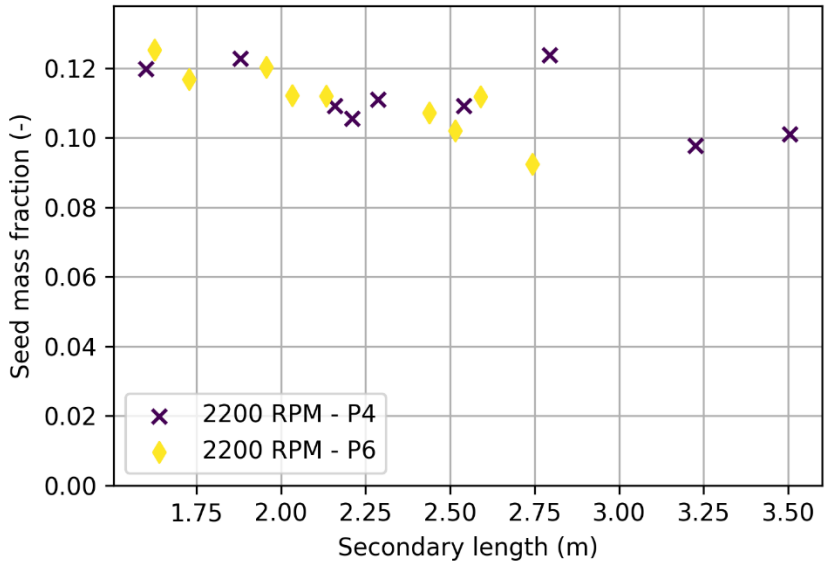

Figure 56. The seed mass fraction results of **Figure 55** plotted against the secondary hose lengths for primary hoses 4 (P4) and 6 (P6) of the modeled full-scale air drill.

A trend of decreased seed mass fraction being conveyed through longer secondary hoses was present in the simulation results for distributors 4 and 6 in **Figure 56**. A stronger sensitivity to secondary hose length appeared in the results for distributor 6. Given the complex geometry of

primary hose 4 upstream of the entry to the distributor, multiple factors likely influenced the distribution pattern. The greatest fraction of seed mass for distributor 4 was conveyed through outlet position 7, which had a secondary hose length of approximately 2.80 m. In contrast, the next two longest hoses, corresponding to outlet positions 4 and 5, respectively, conveyed the lowest seed mass fraction.

7.4 Conclusions from the Simulation of Pneumatic Conveying Systems

Simulating the pneumatic conveying of canola through an air drill began with the development of an air-only CFD model of a primary hose, and eventually a distributor and secondary hoses. The predicted pressure drop was somewhat higher than some experimental results but, in general, the results agreed well with available validation data. The addition of inflation layers to the CFD grid made a significant improvement to the accuracy of the velocity profile through a pipe cross-section in comparison to theory. Therefore, at the cost of computational speed, inflation layers were included throughout the subsequent simulation efforts.

The air-only model of a basic pneumatic conveying system revealed several noteworthy features. Flow separation occurred on the inside of the J-tube elbow even at the lowest fan speed replicated in the simulation, leading to higher-velocity air flowing around the outside of the elbow. However, the dimples in the vertical portion of the J-tube forced the highest velocity air toward the center of the tube to some degree. Thus, the velocity profile of the air was asymmetric from the inside to the outside of the elbow. This caused a structural imbalance of the mass flow rate of air through the nine outlets of the distributor with equal length secondary hoses. More air flowed through the secondary hoses opposite the side of the J-tube elbow, regardless of the simulated fan speed. The mass flow rate evenly transitioned to the lowest mass flow rate - through the secondary hoses on the same side of the distributor from which the primary hose approached (secondary hose position 1). Furthermore, the sharp transition from the vertical distributor pipe to the horizontal secondary hoses caused flow separation to occur at the entry into all secondary hoses.

Modifying the length of the secondary hoses resulted in a shift in air mass flux away from lengthened hoses (20.8% longer) toward shortened hoses (25.4 % shorter). This bias was basically additive to the underlying imbalance present between secondary outlets on the inside of the elbow versus the outside. The ration of maximum to minimum air mass fraction values increased from 1.06 with equal length secondary hoses to 1.22 with unequal length hoses.

The parameters developed through the equal and unequal length secondary hose simulations were used to create a CFD model to represent the full-scale air drill used during testing, based on measurements taken during the testing period. The impact of the routing of primary hoses was apparent from those simulations, as was the impact of the large variation of secondary hose lengths and their positions within the distributors. High-curvature bends immediately upstream of the entry to the J-tube, like that present in primary hose 4, affected the flow pattern

within the J-tube. Conversely, the disturbance from gentle bends further from the J-tube were smoothed out if sufficient distance was provided upstream of the J-tube elbow.

The flow field results were then used with a one-way coupling scheme to simulate the movement of canola particles using the discrete element method. One-way coupling enabled relevant lift and drag aerodynamic forces to be transferred onto each particle in the simulation, but the presence of the canola particles did not affect the airflow solution. Within DEM, collisions between particles and with walls were modeled.

The pattern of seed mass distribution for a distributor with equal length hoses was similar to the single-hose laboratory results. However, the simulated results indicated a greater difference between the maximum seed mass flow through secondary position 1 and minimum seed mass flow through the secondary hoses opposite position 1 (positions 5 and 6 for a distributor with nine outlets). Seed was typically carried along the outside of the J-tube elbow before contacting the first dimple. Seed then either bounced between opposite sides of the vertical tube and preferentially entered secondary hose 1 and its neighbors or were re-entrained into the airflow but were unable to follow the streamline of the highest velocity air flow through secondary hose outlets 5 and 6.

Altering the length of some secondary hoses resulted in significantly less variation in the seed mass flow rate between position 1 and position 5 or 6. Notably, there was not a strong bias in seed flow specifically toward the shorter hoses in these simulations. Qualitatively, this agreed with the results from the single-hose laboratory testing, but more study is warranted. A detailed investigation of particle trajectories through these asymmetric flow fields may highlight the mechanism(s) that reduce the apparent bias in seed mass distribution that occurred with secondary hoses of equal length.

Increasing the air velocity did not have a noticeable impact on the distribution consistency with either equal or unequal length secondary hoses; this conclusion differed from the experimental results from the project.

In simulations based on the geometry of the air drill used during full-scale testing, there was an observed trend between increased secondary hose length and both decreased air and seed mass fluxes. This was clearer in primary hose 6 compared to primary hose 4, as a large bend was present upstream of the entry into the J-tube of distributor 4.

The simulated division of the mass flux of air through the pneumatic conveying system generally was not an indicator of the pattern of the actual division of seed; therefore, seed distribution consistency should really only be based on seed distribution measurements as opposed to inferring distribution consistency directly from airflow patterns.

8. IMPACT ON PRODUCER OPERATIONAL PRACTICES

This project represented a multi-year effort in measuring air drill distribution performance, both in the laboratory and at full scale, in addition to simulating various configurations of pneumatic conveying systems. While several themes from the results point to opportunities for improved design of these systems, within the confines of existing machines the project ultimately highlighted the importance of simple but careful maintenance of air drill pneumatic conveying components and systems.

Consistent secondary hose lengths and resulting pressure drops are important to system performance; however, the interaction between secondary hose length and outlet position is complex. Therefore, the manufacturer suggested hose routings should be followed unless actual performance data suggests otherwise. If seed distribution consistency is in doubt, verifying the actual performance of a drill in the range of operation actually employed by an operator is a small cost, particularly when weighed against modern input commodity prices.

Wherever possible, severe bends should be minimized in both primary and secondary hoses. Introducing sharp bends close to the entry of a J-tube elbow should be avoided when replacing primary hoses. Furthermore, the hose fastening/restraint schemes suggested by manufacturers should be used. Replace damaged or kinked hoses immediately.

In the range of solids loading ratios (SLRs) tested (relatively low when compared to most other seed and fertilizers) with the equipment studied in this project, increasing the fan speed actually worsened the distribution consistency, as opposed to improving it by “promoting more mixing” as is sometimes anecdotally suggested. In the simulation results, distribution consistency was at least no better when the air velocity increased. In the testing conducted for this project, the manufacturer-suggested fan speed provided the most consistent distribution of seed across the air drill. Furthermore, the air mass distribution was generally quite consistent across the range of fan speeds tested for the air drill geometries considered throughout this work. Unless drill-specific information suggests otherwise, the most appropriate fan speed is the one suggested by the manufacturer.

Finally, pneumatic conveying the particular canola seed used under the conditions tested through the particular air drill used during full-scale testing did not result in a reduction in germination from the control sample, and variations in samples taken across the air drill were not evident.

9. RECOMMENDATIONS FOR FUTURE WORK

The data and results developed through the course of this project indicated several opportunities for future work:

1. The reduction in the difference between minimum and maximum seed mass fractions that resulted from unequal secondary hose lengths was surprising; a closer mirroring of the air mass fraction response was expected. These results warrant a closer look, and a detailed analysis of particle trajectories through the resulting asymmetric flow fields that resulted from unequal secondary hose lengths may highlight the mechanism(s) that tended to “smooth out” the front-rear seed distribution bias that was present with secondary hoses of equal length.
2. The data suggest that more optimal hose routings (both primary and secondary) are possible, even within the constraints of current designs. Tight bends in both primary and secondary hoses had an apparent impact on distribution consistency. Furthermore, matching secondary hose lengths to specific distributor outlets may provide improvements to distribution consistency. However, given the complex interaction between secondary hose lengths and positions, improvements should be sought via engineered improvements developed by manufacturers. Owner/operator modifications to pneumatic conveying systems are not recommended.
3. Machinery bouncing and accelerations were not considered, as all testing and simulation results reflected stationary equipment. While our initial hypothesis is that equipment motion would improve mixing of particles in the airstream, the non-linear nature of particle motion may result other distribution trends. An investigation through bench-scale testing or by incorporating motion into simulations is suggested as a first step.
4. Further study of particle-wall DEM interaction parameters that reflect used machinery across a wide range of repair is warranted, as well as particle-particle DEM interaction parameters specific to seeding scenarios including manufacturer-applied seed coating, on-farm or in-field applied seed treatments. One set of nominal interactions was used throughout this work without a sensitivity study conducted.
5. Prior experimental work on full scale air drills (Gieger, 2018) indicated a germination sensitivity for soybeans when pneumatically conveyed through an air seeder. Development of a DEM particle representation of a soybean is suggested to enable simulation of that crop through traveling through a pneumatic conveying system. Because of their dicot structure, understanding the forces applied to the seeds during collisions is of particular interest. Quantifying these forces in relation to seed damage and germination would provide a novel understanding of the care required to convey large dicot-type seeds without damage.

10. REFERENCES

Allam, R. K., & Wiens, H. (1982). An investigation of air seeder component characteristics. *1982 Winter Meeting.* Chicago: American Society of Agricultural Engineers.

Altair Engineering Inc. (2021). EDEM 2021.1. *EDEM User guide*. Troy, Michigan, United States of America.

Altair Engineering Inc. (2021). HyperWorks CFD 2021.1. *HyperWorks CFD 2021.1 User Guide*. Troy, Michigan, United States of America.

Bayati, M., & Johnston, C. (2017). *CFD-DEM investivation of seed clustering in an air seeder with the immersed boundary method.* Grand Prairie: Radix Innovation Corporation.

Bjarnason, T., Stock, W., Hultgreen, G., & Wassermann, J. (2005). *Reducing canola seed damage from metering and air distribution systems.* Humboldt: Prairie Agricultural Machinery Institute.

Boac, J., Casada, M., Maghirang, R., & Harner III, J. (2010). Material and interaction properties of selected grains and oilseeds for modeling discrete particles. *Transactions of the ASABE*, 1201-1216.

Bourges, G., & Medina, M. (2013). Air-seeds flow anlaysis in a distributor head of an "air drill" seeder. *Proceedings 1st international symposium on CFD applications in agriculture* (pp. 259-264). Valencia: International society for horticultural science.

Bourges, G., Eliach, J. J., & Medina, M. A. (2017). Numerical investigation of a seed distributor head for air seeders. *Chemical Engineering Transactions*, 571-576.

Bourges, G., Eliach, J., & Medina, M. (2015). Numerical testing of a distributor head modification of an air drill seeder: A performance comparison with actual model. *XXXVI CIOSTA CIGR V Conference.* St. Petersburg: Commission Internationale del'Organisation Scientifique du Travalen Agriculture.

Chung, C. J. (1969). Mechanical damage to corn in a pneumatic conveying system. Manhattan, Kansas: Kansas State University.

Cousins, J. D., & Noble, S. D. (2017). Simulation of multiphase flow conditions in air seeders for control applications. *CSBE/SCGAB 2017 Annual Conference* (pp. 1-10). Winnipeg: The Canadian Society for Bioengineering.

Ebrahimi, M. (2014). *CFD-DEM modelling of two-phase pneumatic conveying with experimental validation.* Edinburgh: Univeristy of Edinburgh.

Eskin, D., Leonenko, Y., & Vinogradov, O. (2007). An engineering model of dilute polydisperse pneumatic conveying. *Chemical Engineering & Processing*, 247-256.

Ganser, H. H. (1993). A rational approach to drag prediction of spherical and nonspherical particles. *Powder Technology, 77*(2), 143-152.

Gieger, L. (2018). *Air seeder distribution and seed damage for wheat, canola, and soybeans.* Portage la Prairie: Prairie Agricultural Machinery Institue.

Haider , A., & Levenspiel, O. (1989). Drag coefficient and terminal velocity of spherical and nonspherical particles. *Powder Technology, 58*(1), 63-70.

Hossain, M. S. (2014, December). Development of semi-empirical models to measure mass flow rate of solids in an air seeder. University of Saskatchewan.

Hubert, M., & Kalman, H. (2003). Experimental determination of length-dependent saltation velocity in dilute flows. *Powder Technology*, 156-166.

Keep, T. (2016). *Effect of localized velocity increase on overall power consumption and flow characteristics in pneumatic conveying systems.* Saskatoon: University of Saskatchewan.

Klinzing, G. E., Rizk, F., Marcus, R., & Leung, L. S. (2010). *Pneumatic conveying of solids: A theoretical and practical approach.* Springer.

Kumar, V., & Durairaj, C. (2000). Infulence of head geometry on the distributive performance of air-assissted seed drills. *Journal of Agriculturan Engineering Research*, 81-95.

Landry, H. (2018). *Discrete Element Modeling of Porosity Distribution in Grain Bulks (SWDC Ref # 151106-24).* Humboldt: Prairie Agricultural Machinery Institute.

Mills, D. (2016). *Pneumatic conveying design guide.*

Mittal, L. (2016, November). *Identifying the flow conditions in pneumatic conveying of wheat grains through horizontal straight and bent pipe using pressure drop.* Thesis, University of Saskatchewan, Saskatoon. Retrieved December 20, 2022, from https://harvest.usask.ca/bitstream/handle/10388/7695/MITTAL-THESIS-2016.pdf?isAllowed=y&sequence=1

Patwa, A., Ambrose, R., & Casada, M. E. (2016). Discrete element method as an approach to model the wheat milling process. *Powder Technology, 302*, 350-356.

R Core Team. (2021). R: A language and environment. Vienna, Austria. Retrieved from https://www.R-project.org/

Ratnayake, C. (2017). Pneumatic conveying of wheat flour : system optimisation through pilot testing. *18th International Conference on Transport and Sediment of Solid Particles*, (pp. 257-264). Prague.

White, F. M. (2006). *Fluid Mechanics.* Mcgraw-Hill College.

Yatskul, A., Lemiere, J.-P., & Cointault, F. (2017). Influence of the divider head functioning conditions and geometry on the seed's distribution and accuracy of the air-seeder. *Biosystems Engineering*, 120-134.

For further information with regards to this report, please contact:
PAMI@pami.ca

Saskatchewan Test Site
Box 1150
2215 – 8th Avenue
Humboldt, SK S0K 2A0
1-800-567-7264